~~Middle and Late Pleistocene~~ Past climate and continentality inferred from ice wedges at Batagay megaslump in the Northern Hemisphere's most continental region, Yana Highlands, interior Yakutia

Thomas Opel[1,2], Julian B. Murton[1], Sebastian Wetterich[2], Hanno Meyer[2], Kseniia Ashastina[3], Frank Günther[2], Hendrik Grotheer[4], Gesine Mollenhauer[4], Petr P. Danilov[5], Vasily Boeskorov[5], Grigoriy N. Savvinov[5], Lutz Schirrmeister[2]

[1]Permafrost Laboratory, Department of Geography, University of Sussex, Brighton, BN1 9RH, United Kingdom
[2]Alfred Wegener Institute, Helmholtz Centre for Polar and Marine Research, Telegrafenberg A45, 14473 Potsdam, Germany
[3]Senckenberg Research Institute and Natural History Museum, Research Station of Quaternary Palaeontology, 99423 Weimar, Germany
[4]Alfred Wegener Institute, Helmholtz Centre for Polar and Marine Research, Am Handelshafen 12, 27570 Bremerhaven, Germany
[5]Science Research Institute of Applied Ecology of the North, North-East Federal University, 43 Lenin Avenue, Yakutsk 677007, Russia

Correspondence to: Thomas Opel (t.opel@sussex.ac.uk, thomas.opel@awi.de)

Abstract

Ice wedges in the Yana Highlands of interior Yakutia—the most continental region of the Northern Hemisphere—were investigated to elucidate changes in ~~the~~ winter climate and continentality ~~during~~ since the Middle ~~to Late~~ Pleistocene. The Batagay megaslump exposes ice wedges and composite wedges that were sampled from three cryostratigraphic units: the ~~L~~lower ~~sand unit~~Ice Complex of likely pre-Marine Isotope Stage (MIS) 6 age, the ~~upper~~ Upper Ice Complex (Yedoma) and the ~~upper~~ Upper ~~sand~~ Sand unit (both MIS 3 to ~~MIS~~2). A terrace of the nearby Adycha River provides a Late Holocene (MIS 1) ice wedge that serves as a modern ~~endmember~~reference for ~~analysis~~interpretation. The ~~s~~Stable-isotope ~~values~~composition of ice wedges in the MIS 3 ~~upper~~ Upper ~~Yedoma~~Ice Complex at Batagay ~~are~~is more depleted (mean $\delta^{18}O$ about –35‰) than ~~those~~ that from 17 other ice-wedge study sites across coastal and central Yakutia. This observation points to lower winter temperatures and, therefore, higher continentality in the Yana Highlands during MIS 3. Likewise, more depleted isotope values ~~compared to other sites in Yakutia~~ are found in Holocene wedge ice (mean $\delta^{18}O$ about –29‰) compared to other sites in Yakutia. Ice-wedge isotopic signatures of the ~~MIS6 lower~~ Lower ~~sand unit~~ Ice Complex (mean $\delta^{18}O$ about –33‰) and of the MIS 3–2 ~~upper~~ Upper ~~sand~~ Sand unit (mean $\delta^{18}O$ from about –33 to –30‰) are less distinctive regionally. ~~and~~ The latter unit preserves traces of fast formation in rapidly accumulating sand sheets and of post-depositional isotopic fractionation.

1 Introduction

Interior Yakutia is currently the most continental region of the Northern Hemisphere. At Verkhoyansk, the pole of cold of the Northern Hemisphere, mean monthly air temperature ranges exceed 60°C and absolute temperatures ranges can ~~exceed~~ reach 100°C (Lydolph, 1985). Mean annual precipitation is only 155 mm (Lydolph, 1985). Scarce ~~stable~~ stable-isotope data indicate

5 that modern winter precipitation in this region has the most depleted isotopic composition in Siberia (Kurita et al., 2004; Kurita et al., 2005) according to the "continental effect" in stable isotope fractionation, i.e. the farthest distance from the source region (Dansgaard, 1964). However, warm summers enrich stable isotopes in summer precipitation at interior sites compared to coastal sites in the North, which also reflects the strong continentality of interior Yakutia. During Late Pleistocene cold stages, when lower sea level exposed larger areas of continental shelves, interior Yakutia probably experienced even stronger

10 continentality, with further decreased annual precipitation and ~~larger~~ increased annual temperature amplitudes. Such increased amplitudes must have resulted from either lower winter temperatures or higher summer temperatures or a combination of both. ~~Although~~ While biological proxies such as pollen or plant macro~~fossil~~fossil remains can be used to reconstruct summer climate, winter conditions in ~~this region~~interior Yakutia may be inferred only from ice wedges, which ~~are widespread~~can be found in Middle and Late Pleistocene as well as Holocene permafrost deposits. Ice wedges provide winter temperature information due

15 to their specific seasonality, with frost cracking in winter and crack infilling by snowmelt in spring (Opel et al., 2018). They integrate the ~~stable~~ stable-isotope composition of ~~cold~~ cold-season precipitation (Meyer et al., 2015), which in high northern latitudes is mainly a function of temperature (Dansgaard, 1964). However, a knowledge gap exists about the winter palaeoclimate of interior Yakutia, because ice-wedge studies in the Yana Highlands—between the Verkhoyansky and Chersky ranges—began only recently (Vasil'chuk et al., 2017). In contrast, other sites in east ~~Siberian~~ Siberia (west Beringia) ~~sites~~ have

20 been extensively studied over recent decades, including the coastal lowlands to the north (e.g. Meyer et al., 2002a; Meyer et al., 2002b; Opel et al., 2017b), the Kolyma region to the east (e.g. Vasil'chuk et al., 2001; Vasil'chuk, 2013; Vasil'chuk and Vasil'chuk, 2014) as well as central Yakutia to the south (e.g. Popp et al., 2006) (Figure 1). Ice-wedge studies have been carried out also in east Beringia, e.g. in Alaska, Yukon, and Northwest Territories (Kotler and Burn, 2000; Meyer et al., 2010b; Fritz et al., 2012; Lachniet et al., 2012; Porter et al., 2016).

25 Here we report cryostratigraphic field observations of ice wedges and composite wedges made during a reconnaissance expedition from 27 July to 5 August 2017 together with stable-isotope data from the Batagay megaslump and Adycha River floodplain (Figure 1). New radiocarbon ages from organic remains in ice wedges and host sediments ~~from the former~~ help constrain the late Quaternary chronology. The observations and ages elucidate the history of wedge development, past winter temperatures and continentality since ~~MIS 6~~the Middle Pleistocene.

30 **2 Study site characteristics, stratigraphy and chronology**

Neither study site has been glaciated during at least the last 50,000 years, and the Batagay megaslump provides access to permafrost formations since the Middle Pleistocene (Ashastina et al., 2017; Murton et al., 2017). The present mean annual air

temperature at Batagay is −15.4°C (mean of the coldest month: −47.7°C, mean of the warmest month: 15.4°C) and the mean annual precipitation is 170 to 200 mm (Ivanova, 2003). Prevailing wind directions are southwest in winter (January) and north or northeast in summer (July) (Murton et al., 2017). The mean annual temperature of the permafrost is −8.0 to −5.5°C and the active-layer depth between 0.2–0.4 m beneath forest and moss covers and 0.4–1.2 m beneath open sites (Ivanova, 2003).

The **Batagay megaslump** (67.58°N, 134.77°E), close to the city of Batagay on the east bank of the Yana River, is the world's largest known thaw slump (Figure 2) (Ashastina et al., 2017; Murton et al., 2017). It is located on a hillslope in the taiga landscape and exposes a sequence of permafrost deposits at least 60 m thick, with underlying bedrock cropping out in places (Kunitsky et al., 2013). The slump has formed during recent decades (Savvinov et al., 2018), with increasing headwall retreat rates of up to 30 m per year. In 2016 it reached a width of 840 m and a total area of >70 ha (Günther et al., 2016).

The slump exposes Pleistocene and Holocene permafrost formations ranging in age from MIS 6 (or older) to MIS 1 (Ashastina et al., 2017; Murton et al., 2017; Ashastina et al., 2018). Above slate bedrock and a basal diamicton, four major cryostratigraphic units contain ice wedges and/or composite wedges (Figure 3, Table 1). The lowest unit is a pebbly dark sand 3–7 m thick, with ice wedges at least 2–3 m high and 1 m wide truncated by a thaw unconformity. This **Lower Ice Complex** has neither been dated nor sampled previously for wedge ice.

The **Lower Sand** unit above, reaching about 20 m in thickness and is composed of yellowish pore-ice cemented (fine) sand with grey horizontal bands. It contains tall, narrow syngenetic ice wedges up to 0.5 m wide. The middle part of the unit was dated to 142.8±25.3 and >123.2 kyr by optically-stimulated luminescence (OSL) and to 210.0±23.0 kyr by infrared-stimulated luminescence (IRSL) (Ashastina et al., 2017), pointing to its deposition during MIS 6. This age is supported by palaeeocological data (Ashastina et al., 2018). An organic-rich unit of silty sand with abundant wood and plant remains (in lenses up to 3 m thick) overlies a distinct erosional surface near the top of the Lower Sand unit. A wood fragment yielded a conventional radiocarbon age of 49.32±3.15 ¹⁴C kyr BP, outside of the range of calibration (Murton et al., 2017), though palaeoecological analysis points to a Last Interglacial age for the organic material (Ashastina et al., 2018).

The overlying **Upper Ice Complex** is 20–25 m thick and dominated by huge syngenetic ice wedges up to few metres wide and at least several metres high within silty and sandy deposits. Finite radiocarbon ages from 49.0±2.0 ¹⁴C ka BP to 12.66±0.05 ¹⁴C kyr BP (Ashastina et al., 2017) indicate sedimentation gaps or erosive events and reveal a MIS 3 to MIS 2 age for the upper part of the Upper Ice Complex. This unit has numerous chronostratigraphic analogies in the coastal lowlands of northern Yakutia, i.e. the Yedoma Ice Complex (Schirrmeister et al., 2011b; Murton et al., 2015). The Upper Ice Complex forms the highest Pleistocene stratigraphic unit in the upper central part (upslope) of the slump headwall, whereas downslope towards the slump mouth it is overlain and partially grades into the **Upper Sand unit** (Figure 3).

The Upper Sand is up to about 20 m thick and consists of pore-ice cemented brown to grey sand with narrow (≤ 0.5 m wide) syngenetic ice wedges and composite wedges. Radiocarbon ages between 36.30±0.70 ¹⁴C kyr BP and

3

26.18±0.22 ^{14}C ~~ka~~ kyr BP (Ashastina et al., 2017; Murton et al., 2017) indicate deposition during MIS 3 and MIS 2, similar to the ~~upper~~ Upper Ice Complex, but in a more complex spatio-temporal pattern, likely due to varying palaeotopography ~~and~~, sediment supply, and accumulation rates.

A near-surface layer 1–1.5 m thick of brown sand and modern soil covers the sequence. This layer was dated to ~~0.~~295±~~0.0~~30

5   ~~ka~~ ^{14}C yr BP (Ashastina et al., 2017). Distinct (thermo-)erosional contacts can be found between the ~~L~~lower Ice Complex and the ~~lower~~ Lower ~~sand~~Sand, the ~~L~~lower ~~sand~~ Sand and the ~~upper~~ Upper Ice Complex and below the near-surface layer.

According to Murton et al. (2017) exposed floodplains of proximal rivers such as the Bataga~~y~~y and Yana, within 2 and 10 km, respectively, of the slump are the assumed major source of the sediments exposed in the headwall, which implies upslope directed transport by wind. Periglacial~~, proluvial, or~~ and nival processes on nearby hillslopes may also have contributed to

10   sediment supply (Ashastina et al., 2017).

~~The second study site, chosen as a~~For a ~~Late~~ late Holocene reference, we studied an ice wedge at ~~is~~ the actively eroding Holocene to recent bank of a small cut-off channel of the **Adycha River**, about 40 km east of the Batagay megaslump (Figure 1). The Adycha site is located about 3 km upstream of the 60–65 m high and 1.2 km long ~~river~~ river-bluff stratigraphic section at Ulakhan Sullar (Kaplina et al., 1983; Sher et al., 2011; Germonpre et al., 2017). Organic-rich silty sands of alluvial origin

15   are exposed in the Adycha riverbank section.

3 Material and Methods

3.1 Fieldwork

Cryostratigraphic observations of ice wedges, composite wedges, unit contacts and sediments at the Batagay megaslump and a terrace of the Adycha River provided a framework ~~with which we selected samples~~for sample selection. A total of six ice

20   wedges and composite wedges from the ~~L~~lower ~~sand~~Ice Complex, the ~~upper~~ Upper Ice Complex and the ~~upper~~ Upper ~~sand~~ Sand were described in detail and sampled at two sections of the slump (Figures 2, 3). Section 1 was studied in a gully in the icy badlands of the slump~~,~~ (Figure 4), and Section 2 was studied in a headwall slope segment (Figure 5). Composite wedges ~~The~~ of the ~~L~~lower ~~Ice Complex was~~Sand unit were inaccessible due to dangerous outcrop conditions, and no wedges were observed in the near-surface layer. At the Adycha River, we sampled a single ice wedge.

25   Ice samples about 4 cm wide, mostly in horizontal profiles, were obtained by chain saw. Details about the studied ice and composite wedges are given in Table S1. The ice samples were melted on site in sample bags, and the meltwater filled up 30 ml PE bottles that were then ~~then~~ tightly closed and stored cool until stable-isotope analysis.

In addition, water from small streams draining the slump was sampled in several parts of the slump floor and the main outflow stream (n=7) as well as from summer precipitation (n=4). Supernatant water from selected Batagay megaslump sediment

30   samples (n=9) was taken for stable-isotope analysis of intrasedimental pore and segregated ice.

3.2 Stable-isotope analysis

The stable oxygen (δ^{18}O) and hydrogen (δD) isotope ratios of all samples were determined at the Stable Isotope Laboratory of the Alfred Wegener Institute Helmholtz Centre for Polar and Marine Research in Potsdam, using a Finnigan MAT Delta S mass spectrometer with an analytical precision of better than ±0.1‰ for δ^{18}O and ±0.8‰ for δD (Meyer et al., 2000). The

5 isotopic composition is expressed in δ per mille values (‰) relative to the V-SMOW standard. The deuterium excess d was calculated as $d = \delta D - 8 \times \delta^{18}O$ (Dansgaard, 1964). ~~In some cases~~For three of seven studied wedges, samples were excluded from further analysis (five in total, Table S2) on the basis that they were lateral ~~ice wedge~~ samples with high sediment content and/or had isotopic values distinctly different from the wedge centres and similar to host sediments, probably due to exchange processes between wedge ice and host sediments (Meyer et al., 2002a; Meyer et al., 2010a)~~were excluded from further analysis~~.

10 ## 3.3 Radiocarbon dating

Organic material from ice wedges and host sediments was radiocarbon dated at the MICADAS ^{14}C dating facility of the Alfred Wegener Institute Helmholtz Centre for Polar and Marine Research in Bremerhaven. The organic material was subjected to chemical leaching and cleaning following the ABA (acid–base–acid) procedure. Material was first submerged in 1 M HCl (for 30 min at 60 °C) to remove carbonate contamination. Following rinsing with Milli-Q water, samples were submerged in

15 1 M NaOH (for 30 min at 60 °C) to leach out humic acids. The base leaching was repeated for a minimum of 7 times or until no coloring of the solution was evident. Afterwards the material was subjected to a final acid treatment (1 M HCl; 30 min at 60 °C), rinsed to neutral with Milli-Q and dried for a minimum of 12 h at 60 °C. Milli-Q used for cleaning and acid/base solutions was pre-cleaned by liquid–liquid extraction with dichloromethane to remove remaining organic contamination. Samples were packed in tin capsules and combusted individually using an Elementar vario ISOTOPE EA (Elemental

20 Analyzer). If samples were smaller than approximately 200 µgC, the CO_2 produced by combustion with the EA was directly injected into the hybrid ion source of the Ionplus MICADAS using the gas interface system GIS (Fahrni et al., 2013). For larger samples, the CO_2 produced was graphitized using the Ionplus AGE3 system (Automated Graphitization System; (Wacker et al., 2010c). The radiocarbon content of the samples was determined alongside size-matched reference standards (oxalic acid; NIST 4990c) and blanks (phthalic anhydride; Sigma-Aldrich 320065) using the Ionplus MICADAS dating system

25 (Synal et al., 2007; Wacker et al., 2010a), and blank correction and standard normalization were performed using the BATS software (Wacker et al., 2010b). Results are reported as $F^{14}C$ (Reimer et al., 2004) and conventional radiocarbon (^{14}C) ages in years BP. Several analyses yielded lower ^{14}C intensities than the blanks included in the respective sequence. In these cases, results are reported as $F^{14}C_{sample} < F^{14}C_{blanks}$. Conventional ^{14}C ages were calibrated using Oxcal 4.3 (Bronk Ramsey, 2009) based on the IntCAL13 dataset (Reimer et al., 2013).

4 Results

4.1 Batagay megaslump

4.1.1 Field observations of ice wedges

The present study confirms cryostratigraphic observations about ice wedges and composite wedges from earlier studies
(Ashastina et al., 2017; Murton et al., 2017) and provides new observations about ice-wedge ~~ice~~ relationships across contacts
between the cryostratigraphic units, ~~which are~~as ~~outlines~~ outlined below.

In the ~~L~~lower Ice Complex, ice wedges are truncated by a thaw unconformity, though the toes of some narrow syngenetic
composite wedges in the overlying ~~L~~lower ~~sand~~ Sand unit extend down across the contact (Figure S1). A single example of
clear ice sharply overlying the shoulder of an ~~composite~~ice wedge in the ~~L~~lower ~~sand unit~~Ice Complex (B17-IW1, Figure 4)
contained brown plant remains and round, few-mm diameter organic bodies identified as hare droppings. This ice lacked the
foliation characteristic of wedge ice and is interpreted as pool ice.

The basal contact of the ~~L~~lower Ice Complex was not observed.

In the ~~L~~lower and ~~upper~~Upper ~~sand~~Sand units, narrow syngenetic wedges vary in apparent width from a few centimetres to
about 0.5 m. Width commonly varies irregularly with height along individual wedges, sometimes gradually, sometimes
abruptly. Wedge height varies from a few metres to at least 12 m. Wedges tend to be oriented approximately at right angle to
colour bands in the sand, such that wedges in the ~~upper~~Upper ~~sand~~Sand unit—whose bands dip downslope, parallel to the
ground surface—are characteristically subvertical, with their tops inclined downslope (Figure S2). The wedge infills grade
between end members of ice-wedge ice and icy sand wedges, with slightly sandy ice-wedge ice (i.e. composite wedges) the
most common type. ~~A single example of clear ice sharply overlying the shoulder of a composite wedge in the lower sand unit~~
~~(B17-IW1, Figure 4) contained brown plant remains and round, few-mm diameter organic bodies identified as hare droppings.~~
~~This ice lacked the foliation characteristic of wedge ice and is interpreted as pool ice.~~

Near the base of the ~~upper~~Upper Ice Complex, syngenetic ice wedges, a few metres wide tend to narrow downwards in the
lower several metres of the unit and terminate with irregular or flattish or U- to V-shaped toes over a vertical distance of about
1–3 m (Figure S2). At the northeast part of the slump headwall, however, the base of the ~~upper~~Upper Ice Complex is a sharp
contact that cuts down into and truncates bands in the underlying ~~L~~lower ~~sand~~Sand unit over a vertical distance of up to at
least several metres (Figure 3). As a result, the ~~upper~~Upper ~~ice~~Ice ~~complex~~Complex thickens substantially downslope.

The top of the ~~upper~~Upper ~~ice~~Ice ~~complex~~Complex displays a variety of wedge relationships with the overlying ~~upper~~Upper
~~sand~~Sand unit (Figure S3). Some wide syngenetic wedges terminate along planar to gently undulating contacts that are
horizontal to gently dipping and have apparent widths of about 1–3 m; some taper upward into narrow wedges characteristic
of the ~~upper~~Upper ~~sand~~Sand unit; some taper irregularly upward, marked by shoulders up to about 0.5 m wide; and some end
upwards with a narrow offshoot. These changes occur over a vertical distance of about 1–3 m.

4.1.2 Lower ~~sand unit~~Ice Complex (~~pre-~~MIS ~~7~~6)

A small truncated ice wedge B17-IW1 (0.5 m wide, 1.1 m high) from the L~~l~~ower ~~sand unit~~Ice Complex was sampled in section 1 (Figure 4) near the slump bottom, about 50 m below the ground surface (~~and~~ about 5 m below the altitude level in the Lower Sand unit dated by luminescence to 142.8±25.3 and >123.2 ~~ka~~kyr (~~by~~ OSL) and to 210.0±23.0 ~~ka~~kyr ~~by~~ (IRSL) (Ashastina et al., 2017). It shows a mean stable-isotope composition of –33.1‰ for $\delta^{18}O$, –256.7‰ for δD, and 8.0‰ for d ~~excess~~ (n=6), with very little variability (Table ~~1~~2, Figure 6). The regression line in a $\delta^{18}O$–δD bi-plot is $\delta D = 12.78\ \delta^{18}O + 166.23$ ($R^2 = 0.80$).

The isotopic composition of the intrasedimental ice (n=~~4~~2) shows similar mean δ values (–32.~~6~~5‰ for $\delta^{18}O$, –~~244~~247.~~3~~1‰ for δD), but higher d ~~excess~~ values (~~14.7~~12.8‰). The co-isotopic regression line is $\delta D = $ ~~20.06~~4.09 $\delta^{18}O$ +– ~~405.23~~114.27 ~~(R^2 = 0.77)~~.

Radiocarbon dating of twigs, Cyperaceae stems and roots from a sediment sample 0.5 m above the truncated ice wedge yielded nonfinite ages of >53,400 and >37,500 ^{14}C yr BP (Table ~~2~~3). A hare dropping from the ice wedge was dated to 15,792±358 ^{14}C yr BP, which can be only explained by ~~redistribution or~~ contamination with relocated material.

4.1.3 Lower Sand unit (MIS 6)

The isotopic composition of intrasedimental ice (n=2) from the Lower Sand unit shows very little variability (mean –32.3‰ for $\delta^{18}O$, –241.6‰ for δD, 16.6‰ for d (Table 2, Figure 6). The co-isotopic regression line is $\delta D = 1.33\ \delta^{18}O – 198.54$.

4.1.~~3~~4 Upper Ice Complex (MIS ~~3~~2)

Two large syngenetic ice wedges from the overlying ice-rich ~~upper~~ Upper Ice Complex in section 2 (Figure 5) in the southern part of the slump show more depleted isotope values as compared to the ~~lower sand unit~~Lower Ice Complex (Table ~~1~~2, Figure 6). Ice wedge B17-IW6 (about 0.5 m wide, sampled about 26 m below surface) shows a mean isotopic composition of –35.1‰ for $\delta^{18}O$, –269.4‰ for δD, and 11.0‰ for d ~~excess~~ (n=4). The co-isotopic regression is $\delta D = 12.25\ \delta^{18}O + 159.79$ ($R^2 = 0.99$). The mean ~~stable~~ stable-isotope values of ice wedge B17-IW5 (about 1.6 m wide and sampled about 20 m below surface) are –34.9‰ for $\delta^{18}O$, –271.0‰ for δD, and 8.1‰ for d ~~excess~~ (n=12). The regression line in a $\delta^{18}O$–δD bi-plot is $\delta D = 7.41\ \delta^{18}O$ –– 12.36 ($R^2 = 0.99$). The intrasedimental ice data (n=2) show distinctly enriched mean values (–26.2‰ for $\delta^{18}O$, –195.0‰ for δD, 14.5‰ for d ~~excess~~).

Unidentified plant and insect remains from ice wedge B17-IW6 as well as Cyperaceae remains and roots from host sediment at the lowest studied level in section 2, about 26 m below surface, both revealed nonfinite ages (>37,500 ^{14}C yr BP; Table ~~2~~3). At the level of about 20 m bs rootlets from the host sediment yielded ages of >37,500 and 47,550±677 ^{14}C yr BP, whereas unidentified plant remains from within ice wedge B17-IW5 were dated to 24,858±536 ^{14}C yr BP.

4.1.~~4~~5 Upper ~~sand~~ Sand unit (MIS 3-2)

Two narrow sand–ice wedges (composite wedges) and one ice wedge were sampled from the rather ice-poor ~~upper~~ Upper ~~sand~~ Sand unit in section 2 (Figure 5) at the southern part of the slump. Composite wedge B17-IW2 (0.25 m wide) was sampled 2.6 and 2.8 m bs, and composite wedge B17-IW3 (0.2 m wide) was sampled 2.0 m bs. The stable-isotope composition of the composite wedges from the ~~upper~~ Upper ~~sand~~ Sand unit differs from those of ~~both underlying units, i.e.~~ the ~~lower sand unit~~ Lower Ice Complex and the ~~upper~~ Upper Ice Complex (Table ~~1~~2, Figure 6). The mean values are –32.8‰ and –31.9‰ for $\delta^{18}O$, –247.5‰ and –240.5‰ for δD, and 15.1‰ and 14.7‰ for d ~~excess~~ (n=4 and n=2), respectively, and plot well above the Global Meteoric Water Line (GMWL, $\delta D = 8\ \delta^{18}O + 10$) (Craig, 1961)~~)~~. The corresponding regressions are $\delta D = 12.51\ \delta^{18}O + 163.29$ ($R^2 = 0.92$) and $\delta D = 14.47\ \delta^{18}O + 220.91$, respectively.

Ice wedge B17-IW4 (about 0.4 m wide and containing a few thin sand veins) was sampled in the ~~upper~~ Upper ~~sand~~ Sand 2.0 m bs and exhibits a more enriched stable-isotope composition (mean values –29.9‰ for $\delta^{18}O$, –227.8‰ for δD, and 11.6‰ for d ~~excess~~ (n=6). The co-isotopic regression is $\delta D = 15.03\ \delta^{18}O + 222.01$ ($R^2 = 0.91$) (Table ~~1~~2, Figure 6).

The intrasedimental ice (n=3) shows similar mean δ values (–30.6‰ for $\delta^{18}O$, –220.0‰ for δD) but higher d ~~excess~~ (24.4‰) values compared to the composite wedges and the ice wedges of the ~~upper~~ Upper ~~sand~~ Sand. The regression line in a $\delta^{18}O$–δD bi-plot is $\delta D = 10.61\ \delta^{18}O + 104.19$ ($R^2 = 0.99$).

Two radiocarbon ages (analysed as gas) of small samples of *Empetrum nigra* leaf, twigs, and Cyperaceae remains from host sediment about 11 m bs are nonfinite, whereas a graphite target yielded an age of 38,348±236 ^{14}C yr BP.

4.1.~~5~~6 Slump outflow

The samples from the outflow stream draining the slump plot well above the GMWL (Table ~~1~~2, Figure 6). Their average stable-isotope values are –31.7‰ for $\delta^{18}O$, –238.6‰ for δD, and 15.2‰ for d ~~excess~~ ($\delta D = 8.84\ \delta^{18}O + 41.83$ ($R^2 = 0.97$, n=7).

4.1.~~6~~7 Summer precipitation

The samples of summer precipitation from both sites show much more enriched stable-isotope compositions than the wedges, as expected (Table ~~1~~2). The samples taken at the Batagay megaslump plot on a co-isotopic regression line of $\delta D = 7.93\ \delta^{18}O + 1.65$ ($R^2 = 1$). Mean values are –14.3‰ for $\delta^{18}O$, –112.0‰ for δD, and 2.6‰ for d ~~excess~~ (n=4).

4.2 Adycha River

Ice wedge A17-IW3 was about 0.3 m wide and sampled about 1.4 m above river level and about 2 m below the ground surface. Its mean stable isotope values are –29.0‰ for $\delta^{18}O$, –226.3‰ for δD, and 5.5‰ for d ~~excess~~ (n=10, Table ~~1~~2, Figure 6). The regression line in a $\delta^{18}O$–δD bi-plot is $\delta D = 7.01\ \delta^{18}O$ – 23.25 ($R^2 = 0.99$).

Rootlets and larch needles from the host sediment were dated to 213±109 ^{14}C yr BP and confirm the Late Holocene age of the alluvial sediments and the ice wedge.

5 Discussion

5.1 Chronostratigraphy of the Batagay megaslump

To date, the exceptionally long record of permafrost history under highly continental climate conditions as ~~preserved~~ exposed in the Batagay megaslump is still not entirely established in terms of its geochronology. Previous studies by Ashastina et al.

5 (2017) and Murton et al. (2017) provide the general differentiation into four main units with ice and/or composite wedges overlain by Late Holocene cover deposits, which are the ~~L~~lower Ice Complex (pre-MIS 6), the ~~L~~lower ~~sand~~ Sand unit (MIS 7– 6), the ~~upper~~ Upper Ice Complex (MIS 3–2) and the ~~upper~~ Upper ~~sand~~ Sand unit (MIS 3–2). Thaw unconformities as observed in sampled sections of this study (Figure 4, Figure 5), but also in previous studies (Ashastina et al., 2017; Murton et al., 2017) question the ~~completeness~~ chronological continuity of the archive. Such (thermo-)erosional features are often observed in late

10 Quaternary permafrost chronologies (e.g. Wetterich et al., 2009) and most likely caused by intense permafrost degradation during warm stages such as the Last Interglacial with widespread thermokarst (Reyes et al., 2010; e.g. Kienast et al., 2011) or exceptionally warm interstadials, but might also relate to palaeotopography and respective accumulation and erosion areas. The Batagay megaslump, on account of its huge dimensions and rapid erosion, holds potential ~~The Batagay megaslump~~ ~~exposes the single stratigraphic units in different contacts. Its complex structure, the rapid erosion and the huge dimensions,~~

15 ~~however, hold potential~~ to identify additional records and units in future studies. With the present study and additional radiocarbon dating, further confidence of the existing stratigraphy is reached, although the wedge-ice derived age information ~~asks for~~ requires careful interpretation. Due to the formation mechanism and downward directed growth of wedge ice, organic remains from inside the ice are commonly younger than those of the host deposits at the same altitude (i.e. sampling depth). The risk ~~to date~~ of dating redeposited organic material, that entered into or later froze onto the surface of ice recently exposed

20 in a slump, is ~~always given~~ common, in particular in erosional features such as ~~a~~ slump floor ~~with~~ gullies. It can be seen in the truncated **L~~l~~ower ~~sand unit~~Ice Complex** (Figure 4) where an age of about 16 ^{14}C ~~ka~~ kyr BP was obtained from the ice wedge, while radiocarbon dates of the host deposit are infinite and luminescence ages of the overlying Lower Sand unit reach 142.8±25.3 ~~ka~~ kyr and >123.2 ~~ka~~ kyr by OSL as well as 210.0±23.0 ~~ka~~ kyr by IRSL (Ashastina et al., 2017). We therefore excluded this anomalously young radiocarbon age from further interpretation.

25 A distinct ~~layer~~ unit of wood and ~~other~~ plant remains up to ~~1.5~~3 m thick and traceable along the exposure is situated ~~above~~ near the top of the ~~L~~lower ~~sand~~ Sand unit and below the ~~upper~~ Upper Ice Complex. Radiocarbon dating of this layer revealed an infinite radiocarbon age of >44 ^{14}C ~~ka~~ kyr BP (Ashastina et al., 2017) as well as an ~~out~~ out-~~of~~ of-calibration age of 49.32±3.15 ^{14}C ~~ka~~ kyr BP (Murton et al., 2017). The palaeobotanic proxy data indicate a warm climate. The plant macro-fossil record is characterized by considerable species richness (34 species), mainly representing northern Taiga forests, including

30 larch and birch trees, shrub alder and raspberry and further representatives of the taiga's understorey. Hence the unit is aligned to the Last Interglacial (Ashastina et al., 2018), ~~that~~ which caused particular thaw of the underlying ~~L~~lower ~~sand~~ Sand unit and formed a discon~~formity~~rdance~~ in the sequences~~.

The expected difference between ice-hosted and sediment-hosted ages of the same sample depth is clearly seen in the ~~upper~~ **Upper** Ice Complex, where organic remains from the ice wedge are dated to about 25 ^{14}C ~~ka~~ kyr BP and the host deposits yield nonfinite to about 48 ^{14}C ~~ka~~ kyr BP ages (Figure 5). However, even though the age offset is very large and a contamination of the dated sample in the field cannot be fully excluded, such information may be reliable and lies within the previously dated

5 overall accumulation period of the ~~upper~~ Upper Ice Complex between about 49 and 13 ^{14}C ~~ka~~ kyr BP (Ashastina et al., 2017; Murton et al., 2017).

The new radiocarbon ages from the ~~upper~~ **Upper** ~~sand~~ **Sand** unit largely confirm the assumed accumulation period of this unit from about 36 to 26 ^{14}C ~~ka~~ kyr BP (Ashastina et al., 2017; Murton et al., 2017), but predate it by about 2000 years, at least with a date of about 38 ^{14}C ~~ka~~ kyr BP and nonfinite ages of >37.5 ^{14}C ~~ka~~ kyr BP from the host deposits. We note that the ~~upper~~

10 Upper ~~sand~~ Sand unit has been studied at two different sites of the slump in different altitude levels (north-northeast of the central headwall (Ashastina et al., 2017; Murton et al., 2017) and together with the ~~upper~~ Upper Ice Complex more downslope in the southern part of the slump~~,~~ (Figure 2), which complicates the correlation of dating results from different sampling sites. Furthermore, close to our section 2, the ~~upper~~ Upper ~~sand~~ Sand could not clearly be differentiated from the ~~upper~~ Upper Ice Complex during fieldwork in 2014 (Ashastina et al., 2017). Hence, the more or less simultaneous accumulation of both the

15 ~~upper~~ Upper Ice Complex and the ~~upper~~ Upper ~~sand~~ Sand unit during MIS 3–2 but their differing spatial distribution in the slump highlights the importance of palaeo-topography in a hillslope setting and varying sediment sources and velocities of deposition and require future sampling and analysis at higher vertical resolution.

Interestingly, no indications for an ~~upper~~ Upper ~~sand~~ Sand ~~layer~~ unit have been found in the top~~most part~~ of the modern headwall on the upslope part of the slump. Additionally, there are no significant Holocene deposits exposed at all in the upper

20 part of the slump. However, carcasses of *Equus lenensis* and ~~baby~~ juvenile *Bison priscus* (dated to 4.45±0.35 ~~ka~~ ^{14}C BP and 8.22~~15~~ +0.45/-0.40 ~~ka~~ kyr ^{14}C BP, respectively) were found at the exit of the slump (Murton et al., 2017). These observations may be related to (a) the palaeo-topographic situation and transport and deposition regimes of windblown ~~dust~~ material during MIS 3–1, likely decreasing upslope, (b) widespread permafrost degradation since the Late Glacial–Early Holocene transition, and/or (c) changed hydrological and vegetation patterns in the Holocene preventing transport and/or deposition of windblown

25 ~~dust~~ sediment.

The **L**~~l~~ower Ice Complex is not dated so far. Given the dating results of the overlying L~~l~~ower ~~sand~~ Sand unit it ~~may~~ might correspond to the Yukagir Ice Complex from Bol'shoy Lyakhovsky Island, which has been dated by radioisotope disequilibria (^{230}Th/U) in peat to 178±14 kyr, 221±27 ~~ka~~ kyr (Wetterich et al., 2019) and ~~to~~ 201±3 ~~ka~~ kyr (Schirrmeister et al., 2002). Hence this unit most likely has survived ~~two~~ both the last and current interglacials. Dating such an old Ice Complex is challenging as

30 the dating approaches are limited and partly still in development. Independently dated tephra layers have been proven useful to date old permafrost in east Beringia, i.e. in Alaska (Schirrmeister et al., 2016) and in Yukon (Froese et al., 2008). However, no tephra layers have been identified yet in the study region due to the long distance from active volcanos. But with its clearly defined stratigraphy and the access to very old permafrost and ice wedges, the Batagay megaslump may be a suitable site to

evaluate and further develop the ice-wedge dating approaches using [36]Cl/Cl⁻ (Blinov et al., 2009) as well as uranium isotope methods (Ewing et al., 2015).

5.2 Cryostratigraphy at the Batagay megaslump – implications for ice-wedge growth regime

The shape and composition of the wedges in the Batagay megaslump correspond to the assumed genesis of the respective units and may also provide palaeoclimate information (Table ~~3~~4). Both the ~~L~~Lower and ~~upper~~ Upper Ice Complex units are characterized by ice wedges up to several m wide, whereas both the ~~L~~Lower and ~~upper~~ Upper ~~sand~~ Sand units contain tall narrow wedges. The former indicates more stable surface conditions with lower ~~accumulation~~ rates of sand aggradation and sufficient melt water supply during the formation of both Ice Complexes that allowed more horizontal growth of ice wedges. The tall narrow wedges of both sand units, in contrast, point to rapid ~~upslope~~ upslope-directed aeolian deposition of ~~sediments~~ sand and, therefore, a predominant vertical ice-wedge growth in persistent polygonal patterns. The downslope inclination of narrow syngenetic wedges in the ~~upper~~ Upper ~~sand~~ Sand unit indicates upward growth subvertically at right angle to the aggrading depositional (hillslope) surface~~, a hillslope~~. The tall and narrow wedges in the sand units are similar in size and shape to chimney-like sand wedges in thick aeolian sand sheets in the Tuktoyaktuk Coastlands of western Arctic Canada, attributed to rapid aggradation of aeolian sand and rapid wedge growth (Murton and Bateman, 2007). ~~Ice~~ The ~~wedges in the lower sand unit point to moister conditions than the~~ composite wedges in the Lower and ~~upper~~ Upper ~~sand~~ Sand unit~~s, which~~ imply dry conditions with only little melt water supply. However, as most ice wedges exhibit a significant sediment content, a steady supply of windblown sediment and a rather thin snow cover during ice-wedge formation is likely.

At the top of the ~~upper~~ Upper Ice Complex, ice wedges tend to narrow and partly transform into narrow composite wedges of the ~~upper~~ Upper ~~sand~~ Sand unit (Figure S3). This indicates a rather gradual change of the deposition regime towards higher sedimentation rates and possibly lower melt water supply due to drier conditions. Interestingly, the polygonal pattern has not been affected by this change, as indicated by the consistent frost-cracking positions. The upward transition of wedges from the ~~upper~~ Upper ~~ice~~ Ice ~~complex~~ Complex to ~~upper~~ Upper ~~sand~~ Sand unit, however, was interrupted episodically by thaw, producing a number of thaw unconformities at different depths. In contrast, the erosional event truncating the ~~L~~Lower Ice Complex seems to have changed the polygonal pattern in which the ~~L~~Lower ~~sand~~ Sand unit has been deposited.

A major erosional surface attributed to gullying by water flowing down a palaeo-hillslope is inferred from the large concave-up lower contact of the ~~upper~~ Upper ~~ice~~ Ice ~~c~~Complex in the northeast part of the headwall (Figure 3). Numerous gullies on the present hillslope near the megaslump are indicated on satellite images between 1968 and 2010 ~~reported by~~ (Kunitsky et al., 2013), which suggests that gullies are characteristic landforms of such terrain under present environmental conditions. Water is supplied to such gullies by snowmelt in spring and rainfall and melt of ground ice in summer. Erosion of the underlying ~~L~~Lower ~~sand~~ Sand unit provided substantial accommodation space for development of an unusually thick ~~upper~~ Upper ~~i~~ice ~~complex~~ Complex with wide ice wedges above it. Stratigraphically, this erosional surface is at a similar level as the upper woody ~~trash~~ debris layer that is thought to be of last interglacial age (Ashastina et al., 2017; Ashastina et al., 2018), which in turn suggests that the erosion also probably took place during warm (interglacial) conditions.

11

5.3 Yana Highlands' ice-wedge stable isotopes – regional palaeoclimate implications

Unfortunately, no comprehensive modern precipitation stable-isotope data are available for the Yana Highlands. The nearest sites with available data are Zhigansk, about 500 km to the west (Kurita, 2011)~~,~~; Tiksi, about 500 km to the northwest (Kloss, 2008)~~–~~; and Yakutsk, about 650 km to the south (Kloss, 2008; Papina et al., 2017). These sites show similar isotopic characteristics for the cold season (October to March). Mean $\delta^{18}O$ values decrease along the north~~-~~–south transect from about ~~-~~–29‰ in Tiksi to ~~-~~–31‰ in Yakutsk, and d ~~excess~~ varies strongly without a clear geographical pattern and shows values between about 8 and 15‰. In general, the mean winter δ-values~~isotopic data~~ plot around the GMWL. However, these sites are characterized by less cold winters compared to the Yana Highlands. Furthermore, they are located east and south, respectively, of the Verkhoyansky Range (Figure 1), ~~that~~ which constitutes an orographic barrier for atmospheric moisture transport ~~from~~ by the westerlies and thereby contributes to the extreme cold and dry winters of the Yana Highlands. Hence, more depleted $\delta^{18}O$ values can be expected for winter precipitation.

The Yana Highlands' ice-wedge ~~stable~~ stable-isotope data form two major clusters (Figure 6, Table 2). The regression of the first cluster (cluster 1) plots below but mainly parallel to the GMWL ($\delta D = 7.45\ \delta^{18}O - 10.46$, $R^2=1$) ~~(Figure 6)~~ and comprises ice wedges B17-IW1 (~~lower sand unit~~Lower Ice Complex), B17-IW5, B17-IW6 (both ~~upper~~ Upper Ice Complex) and A17-IW3 (recent Adycha riverbank). The regression of the second cluster (cluster 2) plots clearly above the GMWL ($\delta D = 6.88\ \delta^{18}O - 21.72$, $R^2=0.97$) and comprises all data from the ~~upper~~ Upper ~~sand~~ Sand unit (composite wedges B17-IW2, B17-IW3, ice wedge B17-IW4). ~~The sediment-rich ice wedge B17-IW6 (upper Ice Complex) plots in-between the clusters.~~ Furthermore, all except one of the intrasedimental-ice samples as well as all slump outflow samples—interpreted as integrated signal of the entire exposed Batagay sequence—plot well above the GMWL. In summary, the higher the sediment content of our samples, the higher are the d ~~excess~~ values and, hence, the offset above the GMWL. The composite and ice wedges from the Upper Sand unit, likely formed in a generally dry environment (section 5.2), exhibit high d values (cluster 2). In contrast, the ice wedges from cluster 1, likely formed under moister conditions with more abundant melt water supply, show lower d values. This suggests that the divergence from cluster 1 (or the GMWL), i.e. higher d, might be an indicator of drier conditions. ~~Considering the cryostratigraphic interpretation of composite wedge and ice wedge formation, the high d excess values in the wedges from the upper sand unit might also be related to a generally dry environment during sediment deposition and wedge formation, whereas the lower d excess values of the other cluster might point to more abundant melt water supply during ice wedge formation.~~

Generally, the high d ~~excess~~ values indicate a higher kinetic fractionation at the moisture source, e.g. due to initial evaporation under low relative humidity and/or high sea-surface temperature conditions (Pfahl and Sodemann, 2014). As we are dealing with cold-stage MIS 3–2 ground ice, higher sea-surface temperatures are unlikely, whereas a changed moisture source region might be possible. As the cold season in ~~Eastern~~ east Siberia is characterized by higher d ~~excess~~ values than the warm season, one might conclude that ~~cold~~ cold-season precipitation does not only feed the ice and composite wedges but also contributes significantly to the formation of intrasedimental ice. However, secondary fractionation during snow cover evolution under

extremely continental conditions with a generally lower snow cover, and snow melt containing only a fraction of the initial snow, ~~refreezing~~ might also affect *d* preserved in wedge ice (Opel et al., 2018; Grinter et al., 2019). For intrasedimental ice, too, ~~and~~ multiple freeze–thaw cycles in the active layer ~~may also affect *d* excess in wedge and intrasedimental ice~~have to be taken into account.

5 The regional palaeoclimatic implications for the Yana Highlands drawn from our ice-wedge δ¹⁸O data are summarised in Table ~~3~~4 together with palaeoecological results from Ashastina et al. (2018). ~~Extremely~~The lowest winter temperatures of our dataset ~~(δ¹⁸O values around −35‰)~~ are indicated ~~recorded~~ by δ¹⁸O values around –35‰ for~~the~~ ice wedges from the Upper Ice Complex, which ~~has~~ formed during the MIS 3 interstadial (Kargin interstadial in Siberian stratigraphy). Similar values including *d* ~~excess~~ have been reported by Vasil'chuk et al. (2017) for three undated ice wedges from the ~~upper~~ Upper Ice Complex sampled close

10 to the headwall of the Batagay megaslump (Figure 3). ~~Very low winter~~Slightly higher temperatures during the formation of the Lower ~~lower sand unit~~Ice Complex ~~during~~before MIS 6 ~~(Taz stadial)~~ are ~~also~~ indicated by δ¹⁸O values around –33‰. However, given the small size of the corresponding ice wedge, the old age and rather similar isotope values of intrasedimental ice in the host deposits some postdepositional alteration of the originally recorded signal (Meyer et al., 2002a; Meyer et al., 2010a) cannot be excluded. Hence, these values should be treated with caution. ~~Very low to low~~Comparable and slightly higher

15 winter temperatures can be inferred for composite wedges (δ¹⁸O values around –33‰ and –32‰) and an ice wedge (δ¹⁸O values about –30‰) from the ~~upper~~ Upper ~~sand~~ Sand unit, which is attributed to the transition from MIS 3 to ~~MIS~~ 2. Again, similar values have been reported by Vasil'chuk et al. (2017) for an undated narrow ice wedge from the ~~upper~~ Upper ~~sand~~ Sand unit sampled in another part of the Batagay megaslump (Figure 3). However, the palaeoclimatic significance of the rather small composite wedges with few samples has to be treated with caution. Ice wedge B17-IW4 might even be an epigenetic ice

20 wedge of Holocene age, given the quite similar δ¹⁸O values (about –29‰) of the definitively Holocene ice wedge from the Adycha river bank (A17-IW3), which indicate ~~moderate to low~~higher winter temperatures in the last centuries to millennia. These values are close to those of modern winter precipitation at Tiksi, Zhigansk and Yakutsk. As modern ice wedges are ~~there is usually~~ enriched by several ‰ in δ¹⁸O compared to modern winter snow cover ~~an offset between the stable isotope composition of modern snow cover and wedge ice~~ (Grinter et al., 2019; Opel et al., 2018), ~~these values~~we suggest that ~~the~~

25 modern winter precipitation in the Yana Highlands is isotopically distinctly more depleted than that at Tiksi, Zhigansk and Yakutsk.

No palaeoclimatic information based on ice-wedge isotopes is available yet from Batagay for the MIS 4 (Zyryan) and MIS 2 (Sartan) stadials. ~~However, a~~ On~~t~~ Bol'shoy Lyakhovsky Island ~~in northeastern Siberia~~of the New Siberian Archipelago ice wedges from both periods show δ¹⁸O values about 6‰ lower than those of MIS 3 Ice Complex ice wedges (Wetterich et al.,

30 2011; Opel et al., 2017b; Wetterich et al., 2019). Hence, even more depleted δ¹⁸O values ~~of about −40‰ could~~ might be expected in ~~LGM~~ ice wedges of Last Glacial Maximum age at the Batagay megaslump. However, we note that distinctly depleted δ¹⁸O values for MIS 4 and 2 have been found only at Bol'shoy Lyakhovsky Island.

When interpreting ice-wedge stable isotopes in terms of absolute palaeotemperatures one has to keep in mind that the isotopic composition of the oceanic moisture source has changed over glacial-interglacial timescales, with enrichment in δ¹⁸O in the

ocean water during past cold stages. Correcting the ice-wedge stable isotopes for this effect requires detailed knowledge about the moisture source region and in particular a better constrained chronology of ice-wedge isotopes than is available from our dataset.

In general, the inferred lower winter temperatures meet the expectations of an increased continentality during the Late Pleistocene cold stages as well as partly drier conditions indicated by the formation of composite wedges. Palaeoecological analysis (plant macrofossil remains, pollen and beetles) of Batagay megaslump deposits (Ashastina et al., 2018) indicates generally much drier conditions compared to recent times (Table 34), in particular during the cold stages. Tree and beetle indicators imply warm summers for most units, whereas macrofossil remains indicate cold to very cold winters for the upper Upper Ice Complex. These patterns are generally in line with our ice-wedge interpretation and support the hypothesized higher continentality.

5.4 Large-scale implications for palaeoclimate and past continentality

The spatial significance of our data can be considered in terms of the upper Ice Complex of the Batagay megaslump, formed in the MIS3 Kargin interstadial (about 50 to 30 ka ago) as well as the Holocene.

5.4.1 MIS 3 interstadial wedge ice records

To assess the climate and continentality across much of western Beringia during the MIS 3 Kargin interstadial, we compare our Yana Highlands ice-wedge stable-isotope data to a dataset of 17 other ice-wedge sites (Figure 1, Figure 7). Most of the wedges are from the Yedoma Ice Complex (Schirrmeister et al., 2011b; Schirrmeister et al., 2013), which is widely distributed in east and central Siberia. We selected one all available ice wedges per study site in this analysis and only those that provide both $\delta^{18}O$ and d excess data (Table S2S3). Additionally, all except two of the considered wedges or their host sediments have been directly dated by radiocarbon methods to between about 50 and 30 ka kyr ago (MIS 3 interstadial). We appreciate that an ice wedge may not contain a full record of this time period and that the climate was not uniform throughout this period. It is, however, not clear yet whether millennial-scale climate oscillations known from the North Atlantic region (e.g. Dansgaard et al., 1993) also characterized the MIS 3 in east Siberia. Following Murton et al. (2017), there are hints that the MIS 3 in northern areas of northeast Siberia was a time of general climate stability even though the interstadial climate was not monolithic. In particular, a warmer period around 40 ka kyr BP is well known from several palaeoecological proxies for some of the study sites (Wetterich et al., 2014) and from ice wedges of the well dated Bykovsky Peninsula section (Meyer et al., 2002a).

The Batagay upper Upper Ice Complex ice wedge B17-IW5 (and the sediment-rich ice wedge B17-IW6, which has not been included in this analysis as well as the data of Vasil'chuk et al. (2017)) shows $\delta^{18}O$ values of around –-35‰, which is 6 to 2‰ lower than MIS 3 ice-wedge $\delta^{18}O$ data from today's coastal lowlands of northern Yakutia, the Kolyma region and central Yakutia (Figure 8). As hypothesized, the relatively depleted $\delta^{18}O$ values from Batagay clearly point to lower MIS3 winter temperatures during MIS 3 in the Yana Highlands than in the other regionselsewhere, probably due to the more continental

14

location framed by the partially glaciated Verkhoyansky and Chersky ranges. Even the ice-wedge δ^{18}O data from highly continental sites in central Yakutia do not reach such low δdelta values as observed in the Batagay ice wedges. Interestingly, the lowest MIS 3 δ^{18}O values beside Batagay originate from the northeastern-most site, Novaya Sibir' Island. If an Atlantic moisture source for MIS 3 wedge ice is assumed, Novaya Sibir' would represent the farthest location from the source region and therefore show much strongly depleted δ^{18}O values, almost reaching those of Batagay.

The peculiarity of the Yana Highlands is also apparent in the *d* excess data of the MIS 3 ice wedges. The Batagay ice wedges exhibit the highest *d* values, between 8 and 11‰, in the data set. Similar values have been found in ice wedges from central Yakutia, whereas today's coastal lowlands of northern Yakutia, the Laptev Sea islands and the Kolyma region sites show values between 2 and 7‰ (Figure 9). Again, from all northern sites, Novaya Sibir' Island shows the value closest to those of the Yana Highlands and central Yakutia.

Little is known about *d* variation in northeast Siberian ice wedges in general, and particularly within specific time periods. Previous studies have interpreted changes in the *d* values between the Late Pleistocene (low values) and Holocene (higher values) as changes in the moisture sources and transport pathways following the retreat of the Eurasian ice sheets (Meyer et al., 2002a; Meyer et al., 2002b). Higher *d* values in central Yakutia and the Verkhoyansk Mountain forelands have also been found in modern winter snow along a west-to-east transect over eastern Siberia from Yakutsk to Magadan (Kurita et al., 2005). This spatial pattern has been attributed to the influence of different moisture sources, with greater kinetic effects during initial evaporation, as resulting from a lower relative humidity (Kurita et al., 2005). Analogously, during MIS 3, the Yana Highlands and central Yakutia may have received precipitation from other moisture sources and/or transport pathways compared to more northern sites. Due to their more southern location, the Yana Highlands might have received a contribution of moisture from a more southerly source, e.g. the Mediterranean source. Such moisture usually has higher *d* excess values compared to North Atlantic moisture (Gat et al., 2003) and may have reached this region via a different southern moisture transport pathway.

5.4.2 Holocene

The mean δ^{18}O values of the Holocene ice wedge sampled at the Adycha River also point to lower winter temperatures—due to greater continentality—than other Holocene ice wedges in the data set. The Adycha samples (mean δ^{18}O –29‰) are more depleted than Holocene wedges from northeast Siberian coastal sites, which show typically mean δ^{18}O values between –27 and –23‰ (e.g. Meyer et al., 2002b; Meyer et al., 2015; Opel et al., 2017a; Wetterich et al., 2018). Holocene ice wedges from the Bykovsky Peninsula (Meyer et al., 2002a) show exceptional values (mean δ^{18}O of –28 to –26‰), which do not fit into the regional pattern and may be related to local climate or environmental effects. In contrast, Holocene ice wedges from central Yakutia exhibit mean δ^{18}O values of –28 to –26‰ (Popp et al., 2006), which are closer to those from the Yana Highlands and also reflect the greater continentality and lower winter temperatures than the Holocene coastal sites.

The *d* values from Holocene ice wedges in Siberia are highly variable. Mean *d* values at the coastal sites are higher (compared to MIS 3), with values between 4 and 12‰ (e.g. Opel et al., 2011; Meyer et al., 2002b; Wetterich et al., 2008; Wetterich et al., 2018). In contrast, in the Yana Highlands the Late Holocene mean *d* value of 6‰ is lower compared to the MIS 3, whereas

15

Late Holocene *d* values in central Yakutia (between 6 and 11‰) are rather similar to MIS 3 values (Popp et al., 2006). The exceptional ice wedges from the Bykovsky Peninsula (Meyer et al., 2002a) even reach *d* values of 16‰. In summary, Holocene ice ice-wedge *d* excess values do not show a clear spatial pattern that is readily interpreteabled in terms of moisture sources or continentality.

5 **6 Conclusions and outlook**

Our stable-isotope data clearly show that winter temperatures in the Yana Highlands during MIS 3, represented by the upper Upper Ice Complex (Yedoma) at Batagay, and the Holocene were significantly distinctly lower than at other ice-wedge study sites in coastal and central Yakutia. This indicates the persistence of enhanced continentality of the Yana Highlands region during at least part of the Late Pleistocene in western Beringia and during the Holocene. The stable-isotope data from narrow

10 composite wedges of the upper Upper sand Sand unit (MIS 3 - 2) and an old ice wedge from the lower sand unitLower Ice Complex (pre-MIS 6) are less indicative and require additional studies.

High-resolution systematic sampling and dating now needs to be carried out for all cryostratigraphic units of the Batagay permafrost sequence to validate our findings of increased continentality during MIS 3 and the Holocene, to improve the temporal resolution of the Batagay ice-wedge record, and to elucidate the palaeoclimatic history from other time slices. Of

15 particular interest are the lower and uppermost parts of the upper Upper Ice Complex, likely representing MIS 4 and MIS2 stadials, as well as more detailed studies of the yet undated Llower Ice Complex, possibly representing late MIS7 or early MIS6. To establish reliable ice-wedge chronologies for the Upper Ice Complex and Upper Sand unit, radiocarbon dating should include macro remains, dissolved organic carbon and CO_2 from gas bubbles (Lachniet et al., 2012; Kim et al., 2019). Additionally, previous luminescence dating results (Ashastina et al., 2017) need to be validated. Finally, the Batagay

20 megaslump may be an appropriate study site to validate and further develop ice-wedge dating approaches using $^{36}Cl/Cl$ (Blinov et al., 2009) as well as uranium isotope methods (Ewing et al., 2015).

16

Data availability

The ice-wedge and new ^{14}C data will be made available at https://www.pangaea.de after acceptance of this paper.

References

Ashastina, K., Schirrmeister, L., Fuchs, M., and Kienast, F.: Palaeoclimate characteristics in interior Siberia of MIS 6-2: first insights from the Batagay permafrost mega-thaw slump in the Yana Highlands, Climate of the Past, 13, 795-818, 10.5194/cp-13-795-2017, 2017.

Ashastina, K., Kuzmina, S., Rudaya, N., Troeva, E., Schoch, W. H., Römermann, C., Reinecke, J., Otte, V., Savvinov, G., Wesche, K., and Kienast, F.: Woodlands and steppes: Pleistocene vegetation in Yakutia's most continental part recorded in the Batagay permafrost sequence, Quaternary Science Reviews, 196, 38-61, 10.1016/j.quascirev.2018.07.032, 2018.

Blinov, A., Alfimov, V., Beer, J., Gilichinsky, D., Schirrmeister, L., Kholodov, A., Nikolskiy, P., Opel, T., Tikhomirov, D., and Wetterich, S.: Ratio of Cl-36/Cl in ground ice of east Siberia and its application for chronometry, Geochem. Geophys. Geosyst., 10, 12, 10.1029/2009gc002548, 2009.

Bronk Ramsey, C.: Bayesian Analysis of Radiocarbon Dates, Radiocarbon, 51, 337-360, 2009.

Craig, H.: Isotopic variations in meteoric waters, Science, 133, 1702-1703, 1961.

Dansgaard, W.: Stable isotopes in precipitation, Tellus, 16, 436-468, 1964.

Dansgaard, W., Johnsen, S. J., Clausen, H. B., Dahljensen, D., Gundestrup, N. S., Hammer, C. U., Hvidberg, C. S., Steffensen, J. P., Sveinbjornsdottir, A. E., Jouzel, J., and Bond, G.: Evidence for general instability of past climate from a250-kyr ice-core record, Nature, 364, 218-220, 10.1038/364218a0, 1993.

Ewing, S. A., Paces, J. B., O'Donnell, J. A., Jorgenson, M. T., Kanevskiy, M. Z., Aiken, G. R., Shur, Y., Harden, J. W., and Striegl, R.: Uranium isotopes and dissolved organic carbon in loess permafrost: Modeling the age of ancient ice, Geochim. Cosmochim. Acta, 152, 143-165, 10.1016/j.gca.2014.11.008, 2015.

Fahrni, S. M., Wacker, L., Synal, H. A., and Szidat, S.: Improving a gas ion source for C-14 AMS, Nucl Instrum Meth B, 294, 320-327, 10.1016/j.nimb.2012.03.037, 2013.

Fritz, M., Wetterich, S., Schirrmeister, L., Meyer, H., Lantuit, H., Preusser, F., and Pollard, W. H.: Eastern Beringia and beyond: Late Wisconsinan and Holocene landscape dynamics along the Yukon Coastal Plain, Canada, Paleogeogr. Paleoclimatol. Paleoecol., 319, 28-45, 10.1016/j.palaeo.2011.12.015, 2012.

Froese, D. G., Westgate, J. A., Reyes, A. V., Enkin, R. J., and Preece, S. J.: Ancient permafrost and a future, warmer arctic, Science, 321, 1648-1648, 10.1126/science.1157525, 2008.

Gat, J. R., Klein, B., Kushnir, Y., Roether, W., Wernli, H., Yam, R., and Shemesh, A.: Isotope composition of air moisture over the Mediterranean Sea: an index of the air-sea interaction pattern, Tellus Ser. B-Chem. Phys. Meteorol., 55, 953-965, 10.1034/j.1600-0889.2003.00081.x, 2003.

Germonpre, M., Fedorov, S., Danilov, P., Galeta, P., Jimenez, E. L., Sablin, M., and Losey, R. J.: Palaeolithic and prehistoric dogs and Pleistocene wolves from Yakutia: Identification of isolated skulls, J. Archaeol. Sci., 78, 1-19, 10.1016/j.jas.2016.11.008, 2017.

Grinter, M., Lacelle, D., Baranova, N., Murseli, S., and Clark, I. D.: Late Pleistocene and Holocene ice-wedge activity on the Blackstone Plateau, central Yukon, Canada, Quat. Res., 91, 179-193, 10.1017/qua.2018.65, 2019.

Günther, F., Grosse, G., Jones, B. M., Schirrmeister, L., Romanovsky, V. E., and Kunitsky, V.: Unprecedented permafrost thaw dynamics on a decadal time scale: Batagay mega thaw slump development, Yana Uplands, Yakutia, Russia, AGU Fall Meeting, San Francisco, 2016.

Ivanova, R. N.: Seasonal thawing of soils in the Yana River valley, northern Yakutia, 8th International Conference on Permafrost, Zürich, Switzerland, 2003, 479-482, 2003.

Kaplina, T., Kartashova, G., Nikitin, V., and Shilova, G.: New data about sand sequence in the Tuostakh Depression, Byuleten'Komissii po Izucheniyu Chetvertichnogo Perioda (Quaternary Commission Bulletin), 52, 107-122, 1983.

Kienast, F., Wetterich, S., Kuzmina, S., Schirrmeister, L., Andreev, A. A., Tarasov, P., Nazarova, L., Kossler, A., Frolova, L., and Kunitsky, V. V.: Paleontological records indicate the occurrence of open woodlands in a dry inland climate at the present-day Arctic coast in western Beringia during the Last Interglacial, Quaternary Science Reviews, 30, 2134-2159, 10.1016/j.quascirev.2010.11.024, 2011.

Kim, K., Yang, J. W., Yoon, H., Byun, E., Fedorov, A., Ryu, Y., and Ahn, J.: Greenhouse gas formation in ice wedges at Cyuie, central Yakutia, Permafrost Periglacial Process., 30, 48-57, 10.1002/ppp.1994, 2019.

Kloss, A. L.: Water isotope geochemistry of recent precipitation in Central and North Siberia as a proxy for the local and regional climate system. , Diplom, Leibnitz Universität Hannover, 107 pp., 2008.

Kotler, E., and Burn, C. R.: Cryostratigraphy of the Klondike "muck" deposits, west-central Yukon Territory, Can. J. Earth Sci., 37, 849-861, 10.1139/e00-013, 2000.

Kunitsky, V. V., Syromyatnikov, I. I., Schirrmeister, L., Skachov, Y. B., Grosse, G., Wetterich, S., and Grigoriev, M. N.: Ice-rich permafrost and thermal denudation in the Batagay area (Yana Upland, East Siberia), Kriosfera Zemli (Earth Cryosphere), 17, 56-58, 2013.

Kurita, N., Yoshida, N., Inoue, G., and Chayanova, E. A.: Modern isotope climatology of Russia: A first assessment, J. Geophys. Res.-Atmos., 109, 15, 10.1029/2003jd003404, 2004.

Kurita, N., Sugimoto, A., Fujii, Y., Fukazawa, T., Makarov, V. N., Watanabe, O., Ichiyanagi, K., Numaguti, A., and Yoshida, N.: Isotopic composition and origin of snow over Siberia, J. Geophys. Res.-Atmos., 110, 17, 10.1029/2004jd005053, 2005.

Kurita, N.: Origin of Arctic water vapor during the ice-growth season, Geophys. Res. Lett., 38, 5, 10.1029/2010gl046064, 2011.

Lachniet, M. S., Lawson, D. E., and Sloat, A. R.: Revised C-14 dating of ice wedge growth in interior Alaska (USA) to MIS 2 reveals cold paleoclimate and carbon recycling in ancient permafrost terrain, Quat. Res., 78, 217-225, 10.1016/j.yqres.2012.05.007, 2012.

Lydolph, P. E.: The climate of the earth, Roman & Allanheld, Totowa, N.J., 386 pp., 1985.

Magens, D.: Late Quaternary climate and environmental history of the Siberian Arctic – Permafrost Records from Cape Mamontovy Klyk, Laptev Sea, Diplom, Christian-Albrechts-Universität zu Kiel, 106 pp., 2005.

Meyer, H., Schönicke, L., Wand, U., Hubberten, H. W., and Friedrichsen, H.: Isotope studies of hydrogen and oxygen in ground ice - Experiences with the equilibration technique, Isot. Environ. Health Stud., 36, 133-149, 10.1080/10256010008032939, 2000.

Meyer, H., Dereviagin, A. Y., Siegert, C., and Hubberten, H.-W.: Paleoclimate studies on Bykovsky Peninsula, North Siberia-hydrogen and oxygen isotopes in ground ice, Polarforschung, 70, 37-51, 2002a.

Meyer, H., Dereviagin, A. Y., Siegert, C., Schirrmeister, L., and Hubberten, H. W.: Palaeoclimate reconstruction on Big Lyakhovsky Island, North Siberia - Hydrogen and oxygen isotopes in ice wedges, Permafrost Periglacial Process., 13, 91-105, 10.1002/ppp.416, 2002b.

Meyer, H., Schirrmeister, L., Andreev, A., Wagner, D., Hubberten, H. W., Yoshikawa, K., Bobrov, A., Wetterich, S., Opel, T., Kandiano, E., and Brown, J.: Lateglacial and Holocene isotopic and environmental history of northern coastal Alaska - Results from a buried ice-wedge system at Barrow, Quaternary Science Reviews, 29, 3720-3735, 10.1016/j.quascirev.2010.08.005, 2010a.

Meyer, H., Schirrmeister, L., Yoshikawa, K., Opel, T., Wetterich, S., Hubberten, H. W., and Brown, J.: Permafrost evidence for severe winter cooling during the Younger Dryas in northern Alaska, Geophys. Res. Lett., 37, L03501, 10.1029/2009gl041013, 2010b.

Meyer, H., Opel, T., Laepple, T., Dereviagin, A. Y., Hoffmann, K., and Werner, M.: Long-term winter warming trend in the Siberian Arctic during the mid-to late Holocene, Nat. Geosci., 8, 122-125, 10.1038/ngeo2349, 2015.

Murton, J. B., and Bateman, M. D.: Syngenetic sand veins and anti-syngenetic sand wedges, Tuktoyaktuk Coastlands, western Arctic Canada, Permafrost Periglacial Process., 18, 33-47, 10.1002/ppp.577, 2007.

Murton, J. B., Goslar, T., Edwards, M. E., Bateman, M. D., Danilov, P. P., Savvinov, G. N., Gubin, S. V., Ghaleb, B., Haile, J., Kanevskiy, M., Lozhkin, A. V., Lupachev, A. V., Murton, D. K., Shur, Y., Tikhonov, A., Vasil'chuk, A. C., Vasil'chuk, Y. K., and Wolfe, S. A.: Palaeoenvironmental Interpretation of Yedoma Silt (Ice Complex) Deposition as Cold-Climate Loess, Duvanny Yar, Northeast Siberia, Permafrost Periglacial Process., 26, 208-288, 10.1002/ppp.1843, 2015.

5 Murton, J. B., Edwards, M. E., Lozhkin, A. V., Anderson, P. M., Savvinov, G. N., Bakulina, N., Bondarenko, O. V., Cherepanova, M. V., Danilov, P. P., Boeskorov, V., Goslar, T., Grigoriev, S., Gubin, S. V., Korzun, J. A., Lupachev, A. V., Tikhonov, A., Tsygankova, V. I., Vasilieva, G. V., and Zanina, O. G.: Preliminary paleoenvironmental analysis of permafrost deposits at Batagaika megaslump, Yana Uplands, northeast Siberia, Quat. Res., 87, 314-330, 10.1017/qua.2016.15, 2017.

Opel, T., Dereviagin, A. Y., Meyer, H., Schirrmeister, L., and Wetterich, S.: Palaeoclimatic Information from Stable Water 10 Isotopes of Holocene Ice Wedges on the Dmitrii Laptev Strait, Northeast Siberia, Russia, Permafrost Periglacial Process., 22, 84-100, 10.1002/ppp.667, 2011.

Opel, T., Laepple, T., Meyer, H., Dereviagin, A., and Wetterich, S.: Northeast Siberian ice wedges confirm Arctic winter warming over the past two millennia, The Holocene, 27, 1789-1796, 10.1177/0959683617702229, 2017a.

Opel, T., Wetterich, S., Meyer, H., Dereviagin, A. Y., Fuchs, M. C., and Schirrmeister, L.: Ground-ice stable isotopes and 15 cryostratigraphy reflect late Quaternary palaeoclimate in the Northeast Siberian Arctic (Oyogos Yar coast, Dmitry Laptev Strait), Climate of the Past, 13, 587-611, 10.5194/cp-13-587-2017, 2017b.

Opel, T., Meyer, H., Wetterich, S., Laepple, T., Dereviagin, A., and Murton, J.: Ice wedges as archives of winter paleoclimate: A review, Permafrost Periglacial Process., 29, 199-209, 10.1002/ppp.1980, 2018.

Papina, T., Malygina, N., Eirikh, A., Galanin, A., and Zheleznyak, M.: Isotopic composition and sources of atmospheric 20 precipitation in central Yakutia, Earth's Cryosphere, 21, 52-61, 10.21782/EC2541-9994-2017-1(52-61), 2017.

Pfahl, S., and Sodemann, H.: What controls deuterium excess in global precipitation?, Climate of the Past, 10, 771-781, 10.5194/cp-10-771-2014, 2014.

Popp, S., Diekmann, B., Meyer, H., Siegert, C., Syromyatnikov, I., and Hubberten, H. W.: Palaeoclimate signals as inferred from stable-isotope composition of ground ice in the Verkhoyansk foreland, Central Yakutia, Permafrost Periglacial Process., 25 17, 119-132, 10.1002/ppp.556, 2006.

Porter, T. J., Froese, D. G., Feakins, S. J., Bindeman, I. N., Mahony, M. E., Pautler, B. G., Reichart, G. J., Sanborn, P. T., Simpson, M. J., and Weijers, J. W. H.: Multiple water isotope proxy reconstruction of extremely low last glacial temperatures in Eastern Beringia (Western Arctic), Quaternary Science Reviews, 137, 113-125, 10.1016/j.quascirev.2016.02.006, 2016.

Reimer, P. J., Brown, T. A., and Reimer, R. W.: Discussion: Reporting and calibration of post-bomb C-14 data, Radiocarbon, 30 46, 1299-1304, 2004.

Reimer, P. J., Bard, E., Bayliss, A., Beck, J. W., Blackwell, P. G., Bronk Ramsey, C., Buck, C. E., Cheng, H., Edwards, R. L., Friedrich, M., Grootes, P. M., Guilderson, T. P., Haflidason, H., Hajdas, I., Hatte, C., Heaton, T. J., Hoffmann, D. L., Hogg, A. G., Hughen, K. A., Kaiser, K. F., Kromer, B., Manning, S. W., Niu, M., Reimer, R. W., Richards, D. A., Scott, E. M.,

Southon, J. R., Staff, R. A., Turney, C. S. M., and van der Plicht, J.: IntCal13 and Marine13 Radiocarbon Age Calibration Curves 0–50,000 Years cal BP, Radiocarbon, 55, 1869-1887, 2013.

Reyes, A. V., Froese, D. G., and Jensen, B. J. L.: Permafrost response to last interglacial warming field evidence from non-glaciated Yukon and Alaska, Quaternary Science Reviews, 29, 3256-3274, 10.1016/j.quascirev.2010.07.013, 2010.

5 Savvinov, G. N., Danilov, P. P., Petrov, A. A., Makarov, V. S., Boeskorov, V. S., and Grigoriev, S. E.: Environmental Problems of the Verkhoyansky Region, Vestnik of North-eastern Federal University, 6, 19-33, 10.25587/SVFU.2018.68.21798, 2018.

Schirrmeister, L., Oezen, D., and Geyh, M. A.: Th-230/U dating of frozen peat, Bol'shoy Lyakhovsky Island (Northern Siberia), Quat. Res., 57, 253-258, 10.1006/qres.2001.2306, 2002.

Schirrmeister, L., Grosse, G., Schwamborn, G., Andreev, A. A., Meyer, H., Kunitsky, V. V., Kuznetsova, T. V., Dorozhkina,
10 M. V., Pavlova, E. Y., Bobrov, A. A., and Oezen, D.: Late Quaternary History of the Accumulation Plain North of the Chekanovsky Ridge (Lena Delta, Russia): A Multidisciplinary Approach, Polar Geography, 27, 277-319, 10.1080/789610225, 2003.

Schirrmeister, L., Grosse, G., Schnelle, M., Fuchs, M., Krbetschek, M., Ulrich, M., Kunitsky, V., Grigoriev, M., Andreev, A., Kienast, F., Meyer, H., Babiy, O., Klimova, I., Bobrov, A., Wetterich, S., and Schwamborn, G.: Late Quaternary
15 paleoenvironmental records from the western Lena Delta, Arctic Siberia, Paleogeogr. Paleoclimatol. Paleoecol., 299, 175-196, 10.1016/j.palaeo.2010.10.045, 2011a.

Schirrmeister, L., Kunitsky, V., Grosse, G., Wetterich, S., Meyer, H., Schwamborn, G., Babiy, O., Derevyagin, A., and Siegert, C.: Sedimentary characteristics and origin of the Late Pleistocene Ice Complex on north-east Siberian Arctic coastal lowlands and islands - A review, Quat. Int., 241, 3-25, 10.1016/j.quaint.2010.04.004, 2011b.

20 Schirrmeister, L., Froese, D., Tumskoy, V., Grosse, G., and Wetterich, S.: Yedoma: Late Pleistocene Ice-Rich Syngenetic Permafrost of Beringia, in: Encyclopedia of Quaternary Science (Second Edition), edited by: Elias, S. A., Elsevier, Amsterdam, 542-552, 2013.

Schirrmeister, L., Meyer, H., Andreev, A., Wetterich, S., Kienast, F., Bobrov, A., Fuchs, M., Sierralta, M., and Herzschuh, U.: Late Quaternary paleoenvironmental records from the Chatanika River valley near Fairbanks (Alaska), Quaternary Science
25 Reviews, 147, 259-278, 10.1016/j.quascirev.2016.02.009, 2016.

Schirrmeister, L., Schwamborn, G., Overduin, P. P., Strauss, J., Fuchs, M. C., Grigoriev, M., Yakshina, I., Rethemeyer, J., Dietze, E., and Wetterich, S.: Yedoma Ice Complex of the Buor Khaya Peninsula (southern Laptev Sea), Biogeosciences, 14, 1261-1283, 10.5194/bg-14-1261-2017, 2017.

Sher, A. V., Weinstock, J., Baryshnikov, G. E., Davydov, S. P., Boeskorov, G. G., Zazhigin, V. S., and Nikolskiy, P. A.: The
30 first record of "spelaeoid" bears in Arctic Siberia, Quaternary Science Reviews, 30, 2238-2249, 10.1016/j.quascirev.2010.10.016, 2011.

Strauss, J.: Late Quaternary environmental dynamics at the Duvanny Yar key section, Lower Kolyma, East Siberia, Diplom, Universität Potsdam, 108 pp., 2010.

Synal, H. A., Stocker, M., and Suter, M.: MICADAS: A new compact radiocarbon AMS system, Nucl Instrum Meth B, 259, 7-13, 10.1016/j.nimb.2007.01.138, 2007.

Vasil'chuk, Y., and Vasil'chuk, A.: Spatial distribution of mean winter air temperatures in Siberian permafrost at 20-18ka BP using oxygen isotope data, Boreas, 43, 678-687, 10.1111/bor.12033, 2014.

Vasil'chuk, Y. K., Vasil'chuk, A. C., Rank, D., Kutschera, W., and Kim, J. C.: Radiocarbon dating of δ18O-δD plots in Late Pleistocene ice-wedges of the Duvanny Yar (Lower Kolynia River, Northern Yakutia), Radiocarbon, 43, 541-553, 2001.

Vasil'chuk, Y. K.: Syngenetic Ice Wedges: Cyclical Formation, Radiocarbon Age and Stable Isotope Records by Yurij K. Vasil'chuk, Moscow University Press, Moscow, 2006. 404pp. ISBN 5-211-05212-9, Permafrost Periglacial Process., 24, 82-93, 10.1002/ppp.1764, 2013.

Vasil'chuk, Y. K., Vasil'chuk, J. Y., Budantseva, N. A., Vasil'chuk, A. K., and Trishin, A. Y.: Isotope-geochemical characteristics of the Batagay Yedoma (Preliminary results), Arktika i Antarktika (Arctic and Antarctica), 1, 69-98, 2017.

Wacker, L., Bonani, G., Friedrich, M., Hajdas, I., Kromer, B., Nemec, M., Ruff, M., Suter, M., Synal, H. A., and Vockenhuber, C.: MICADAS: Routine and High-Precision Radiocarbon Dating, Radiocarbon, 52, 252-262, 2010a.

Wacker, L., Christl, M., and Synal, H. A.: Bats: A new tool for AMS data reduction, Nucl Instrum Meth B, 268, 976-979, 10.1016/j.nimb.2009.10.078, 2010b.

Wacker, L., Nemec, M., and Bourquin, J.: A revolutionary graphitisation system: Fully automated, compact and simple, Nucl Instrum Meth B, 268, 931-934, 10.1016/j.nimb.2009.10.067, 2010c.

Wetterich, S., Kuzmina, S., Andreev, A. A., Kienast, F., Meyer, H., Schirrmeister, L., Kuznetsova, T., and Sierralta, M.: Palaeoenvironmental dynamics inferred from late Quaternary permafrost deposits on Kurungnakh Island, Lena Delta, Northeast Siberia, Russia, Quaternary Science Reviews, 27, 1523-1540, 10.1016/j.quascirev.2008.04.007, 2008.

Wetterich, S., Schirrmeister, L., Andreev, A. A., Pudenz, M., Plessen, B., Meyer, H., and Kunitsky, V. V.: Eemian and Late Glacial/Holocene palaeoenvironmental records from permafrost sequences at the Dmitry Laptev Strait (NE Siberia, Russia), Paleogeogr. Paleoclimatol. Paleoecol., 279, 73-95, 10.1016/j.palaeo.2009.05.002, 2009.

Wetterich, S., Rudaya, N., Tumskoy, V., Andreev, A. A., Opel, T., Schirrmeister, L., and Meyer, H.: Last Glacial Maximum records in permafrost of the East Siberian Arctic, Quaternary Science Reviews, 30, 3139-3151, 10.1016/j.quascirev.2011.07.020, 2011.

Wetterich, S., Tumskoy, V., Rudaya, N., Andreev, A. A., Opel, T., Meyer, H., Schirrmeister, L., and Huls, M.: Ice Complex formation in arctic East Siberia during the MIS3 Interstadial, Quaternary Science Reviews, 84, 39-55, 10.1016/j.quascirev.2013.11.009, 2014.

Wetterich, S., Schirrmeiste, L., Nazarova, L., Palagushkina, O., Bobrov, A., Pogosyan, L., Savelieva, L., Syrykh, L., Matthes, H., Fritz, M., Gunther, F., Opel, T., and Meyer, H.: Holocene thermokarst and pingo development in the Kolyma Lowland (NE Siberia), Permafrost Periglacial Process., 29, 182-198, 10.1002/ppp.1979, 2018.

Wetterich, S., Rudaya, N., Kuznetsov, V., Maksimov, F., Opel, T., Meyer, H., Günther, F., Bobrov, A., Raschke, E., Zimmermann, H. H., Strauss, J., Fuchs, M., and Schirrmeister, L.: Ice Complex formation on Bol'shoy Lyakhovsky Island (New Siberian Archipelago, East Siberian Arctic) since about 200 ka, Quat. Res., 10.1017/qua.2019.6, 2019.

5

Table 1. Cryostratigraphic units of the Batagay megaslump as presented by Ashastina et al. (2017) and Murton et al. (2017) and the reconciled stratigraphic framework used in this study and proposed for future studies.

Ashastina et al. (2017)		Murton et al. (2017)		This study
Unit	**Description**	**Unit**	**Description**	**Unit**
Unit I	Active layer	Unit 6	Near-surface sand	Near-surface layer
Unit II	Yedoma Ice Complex	Unit 5	Upper sand	Upper Sand
		Unit 4	Upper Ice Complex	Upper Ice Complex
Unit III	Organic-rich layer	Woody lens	Woody lens	Wood and plant remains
Unit IV	Layered brown sands	Unit 3	Lower sand	Lower Sand
Unit V	Ancient Ice Complex	Unit 2	Lower Ice Complex	Lower Ice Complex
-	-	Unit 1	Diamicton	Diamicton

Table 12. Stable isotope ($\delta^{18}O$, δD and *d*-~~excess~~) minimum, mean and maximum values, standard deviations as well as slopes and intercept in the $\delta^{18}O$–δD diagram for all ice and composite wedges, intrasedimental ice, outflow water and rain water, respectively.

Ice wedge/ Type of water	Width (m)	Samples (n)	$\delta^{18}O$ min (‰)	$\delta^{18}O$ mean (‰)	$\delta^{18}O$ max (‰)	$\delta^{18}O$ sd (‰)	δD min (‰)	δD mean (‰)	δD max (‰)	δD sd (‰)	*d* min (‰)	*d* mean (‰)	*d* max (‰)	*d* sd (‰)	Slope	Intercept	R^2
Batagay megaslump																	
Upper ~~sand~~ Sand unit																	
B17-IW2 (CW)	0.25	4	-33.04	-32.83	-32.47	0.25	-250.2	-247.5	-242.8	3.3	13.7	15.1	16.9	1.5	12.51	163.29	0.92
B17-IW3 (CW)	0.2	2	-32.14	-31.87	-31.60	0.38	-244.2	-240.3	-236.4	5.5	12.9	14.7	16.4	2.4	14.47	220.91	1.00
B17-IW4	0.4	6	-30.10	-29.93	-29.71	0.13	-229.6	-227.8	-223.9	2.2	10.0	11.6	13.8	1.3	15.03	222.01	0.82
Intrased. ice	n/a	3	-32.61	-30.55	-29.21	1.82	-242.2	-220.0	-207.3	19.3	18.7	24.4	28.2	5.1	10.61	104.19	0.99
Upper Ice Complex																	
B17-IW5	1.6	12	-36.17	-34.89	-33.50	0.86	-280.6	-271.0	-260.8	6.4	6.8	8.1	10.3	0.9	7.41	-12.36	0.99
B17-IW6	0.5	4	-35.52	-35.05	-34.27	0.57	-274.9	-269.4	-259.7	7.0	8.5	11.0	14.4	2.5	12.25	159.79	0.99
Intrased. ice	n/a	2	-27.63	-26.19	-24.75	2.04	-198.5	-195.0	-191.5	5.0	6.5	14.5	22.5	11.3	2.44	-131.03	1.00
Lower Sand unit																	
Intrased. ice	n/a	2	-32.31	-32.28	-32.24	0.05	-241.6	-241.6	-241.6	0.1	16.4	16.6	16.8	0.3	1.33	-198.54	1.00
Lower ~~sand unit~~ Ice Complex																	
B17-IW1	0.5	6	-33.18	-33.09	-32.91	0.10	-258.3	-256.7	-254.8	1.5	6.9	8.0	9.4	0.8	12.78	166.23	0.80
Intrased. ice	n/a	4→2	-32.56	-32.38 / -32.48	-32.24 / -32.39	0.14 / 0.13	-247.4	-244.3 / -247.1	-241.6 / -246.7	3.2 / 0.5	12.4	14.7 / 12.8	16.8 / 13.1	2.3 / 0.5	20.06 / 4.09	405.23 / 114.27	0.77 / 1.00
Other																	

Outflow water	n/a	7	-32.29	-31.73	-31.35	0.34	-244.0	-238.6	-235.4	3.1	14.3	15.2	16.1	0.6	8.84	41.83	0.97
Rain water	n/a	4	-16.82	-14.33	-10.17	2.92	-131.7	112.0	-79.0	23.1	2.3	2.6	2.9	0.2	7.93	1.65	1.00
Adycha River																	
Holocene river bank Adycha River																	
A17-IW3	0.3	10	-30.40	-28.98	-28.15	0.74	-236.6	-226.3	-220.5	5.2	4.4	5.5	7.3	0.9	7.01	-23.25	0.99
Ice-wedge cluster																	
Cluster 1	(B17-IW1, B17-IW5, B17-IW6, A17-IW3)														7.45	-10.46	1.00
Cluster 2	(B17-IW2, B17-IW3, B17-IW4)														6.88	-21.72	0.97

5

Table 23. Radiocarbon ages of organic remains in ice wedges (sample ID includes IW) and host sediments of the Batagay megaslump and at the Adycha River. The samples were radiocarbon dated as gas targets (Lab ID ends with 1.1) and graphite targets (Lab ID ends with 2.1).

| Sample ID	Depth (m bs)	Lab ID	$F^{14}C$	Radiocarbon age (yr BP)	Calibrated age 95.4% (cal yr b2k)	Dated material	Remarks
Batagay megaslump							
Upper sand Sand unit							
B17-S2-AMS4-1	11	1689.1.1	<0.0094	>37,500	n/a	*Empetrum nigra* leaf, twigs, Cyperaceae remains (sediment)	
		1689.2.1	0.0084±0.0002	38,348±236	42,863—42,140		
B17-S2-AMS4-2	11	1690.1.1	<0.0094	>37,500	n/a	Cyperaceae stems and roots (sediment)	
Upper Ice Complex							
B17-IW5-02	20.3	1684.1.1	0.0453±0.0030	24,858±536	30,355—27,926	unidentified plant remains (ice wedge)	
B17-IW6-04	25.8	1686.1.1	<0.0094	>37,500	n/a	unidentified plant and insect remain (ice wedge)	
B17-S2-AMS5	20.3	1691.1.1	<0.0094	>37,500	n/a	leaf fragment, roots (sediment)	
		1691.2.1	0.0027±0.0002	47,550±677	>50,033		
B17-S2-AMS6	25.8	1692.1.1	<0.0094	>37,500	n/a	Cyperaceae remains, roots (sediment)	
Lower sand unit Ice Complex							
B17-IW1-04	~50	1683.1.1	0.1400±0.0062	15,792±358	20,044—18,402	hare dropping (ice wedge)	Likely redistributed
B17-S1-AMS2	~49.5	1688.1.1	<0.0094	>37,500	n/a	twigs, Cyperaceae stems and roots (sediment)	
		1688.2.1	<0.0013	>53,400	n/a		
Adycha River							
Holocene river bank Adycha River							
A17-K-03	2	1687.1.1	0.9738±0.0132	213±109	<514	rootlets and *larix Larix* needle (sediment)	

5

Table 34. Summary table on of past climate in the Yana Highlands. Palaeoecological interpretations are from (Ashastina et al., 2018) and based on fieldwork in 2014.

| Unit Ice wedge Chronology	Cryostratigraphy	Interpretation	IW isotopes	Interpretation	Palaeoecological interpretation
Adycha, river bank Ice wedge A17-IW3 Late Holocene to recent	Narrow ice wedge, little sediment	Moist (high melt water supply)	δ^{18}O: −29‰ d-excess: 7‰	Cold wintersand rather moist winters	-
Batagay, upper Upper sand Sand unit Composite wedges B17-IW2 /3 MIS 3 /2	Narrow composite wedges	Dry (little snow melt water) and/or high sediment supply	δ^{18}O: −33‰, −32‰ d-excess: 15‰	Dry winters colder than in the Holocene Very cold to cold winters dry winters	Dry summers, T_{july} >12°C (trees)
Batagay, upper Upper sand Sand unit Ice wedge B17-IW4 MIS 3 /2	Narrow ice wedge, little to medium sediment content	Rather moist (higher melt water supply compared to composite wedges)	δ^{18}O: −30‰ d-excess: 12‰	Cold and rather dry winters rather dry winters (Epigenetic Holocene IW?)	Dry summers, T_{july} >12°C (trees)
Batagay, upper Upper Ice Complex Ice wedge B17-IW5 MIS 3	Wide ice wedge, little to medium sediment content	(rather) moist (high melt water supply)	δ^{18}O: −35‰ d-excess: 8‰	Coldest and Extremely cold winters rather moist winters	Dry and (very) warm summers, very cold and dry winters (beetles)
Batagay, upper Upper Ice Complex Ice wedge B17-IW6 MIS 3	Medium ice wedge, high sediment content	Rather dry (drier than IW5, moister than IWs 2/3)	δ^{18}O: −35‰ d-excess: 11‰	Coldest and Extremely cold winters rather dry winters	Dry summers, cold winters
Batagay, lower Lower sand unitIce Complex Ice wedge B17-IW1 Pre-MIS 6	Narrow ice wedge, little sediment content	Moist, high melt water supply	δ^{18}O: −33‰ d-excess: 8‰	Very cold wintersWinters warmer than in MIS 3 and rather moist winters	Dry summers, T_{july} >12°C (trees)
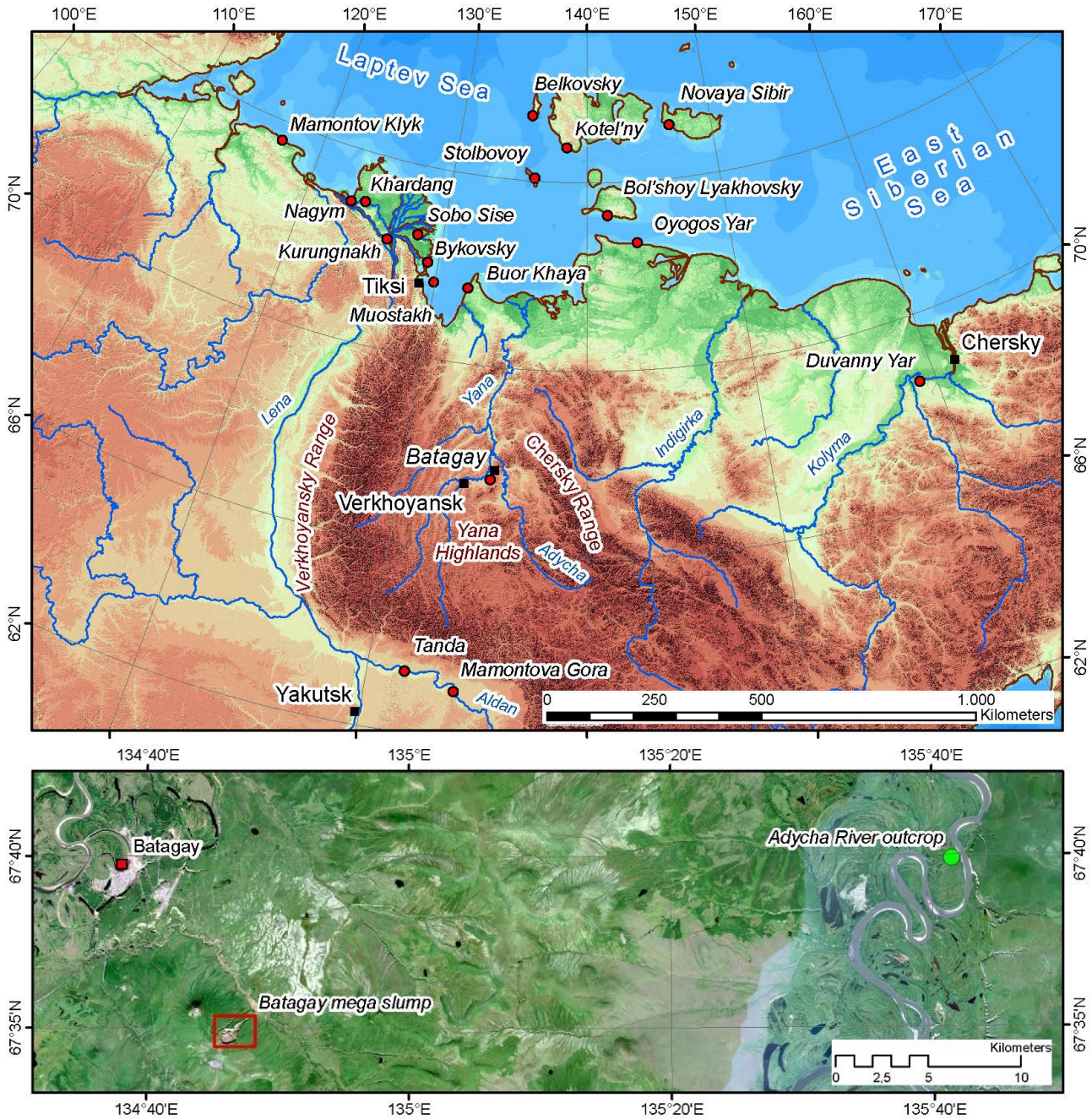
Figure 1. (top) ~~Study~~ Location map of study region in northeastern Siberia showing all ice-wedge study sites mentioned. (bottom) Study sites in the Yana Highlands (Background image: Sentinel-2 mosaic, August 7, August 21, 2017).

5
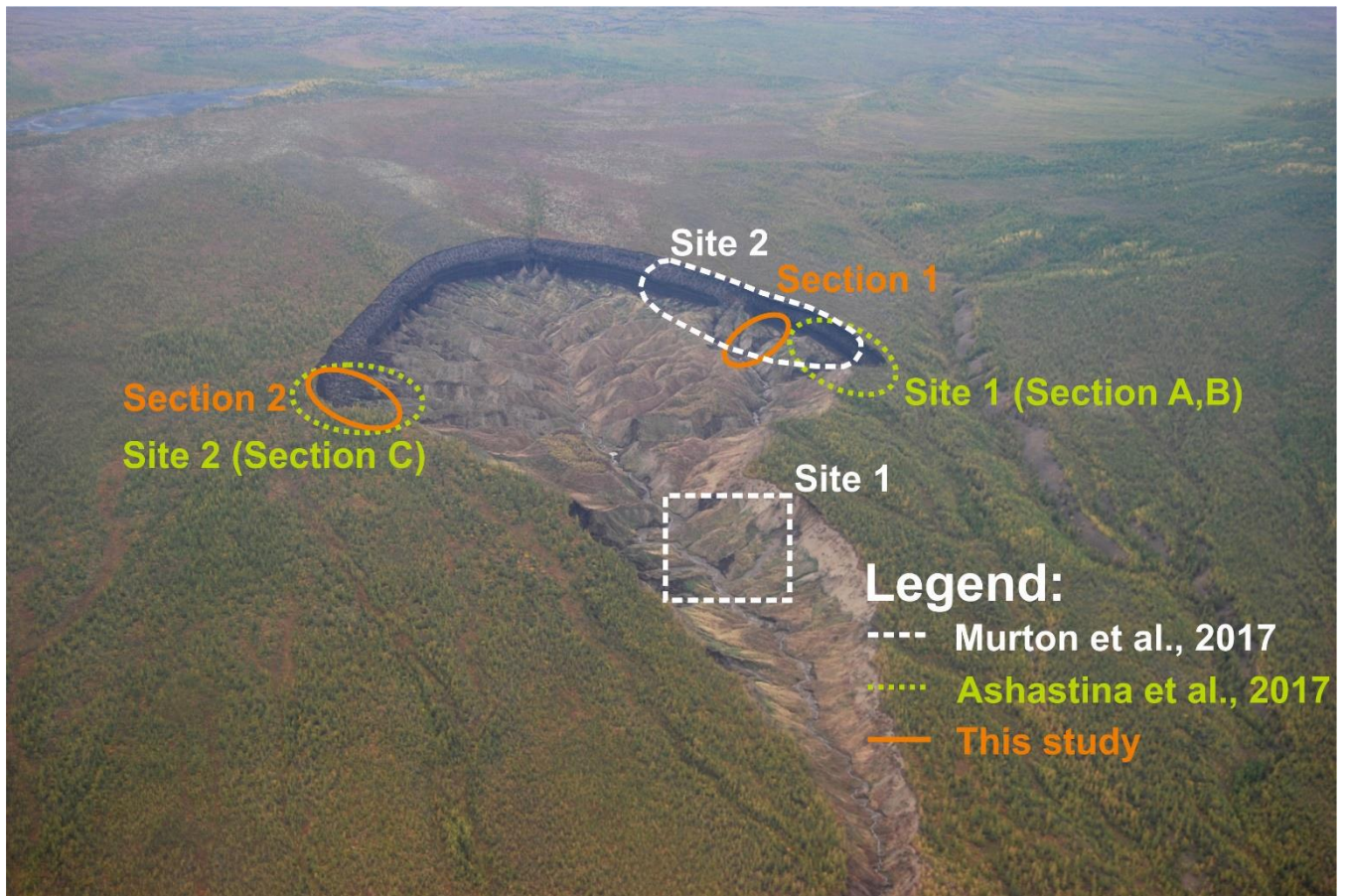
Figure 2. Overview photograph of the Batagay megaslump showing the study sites of (Ashastina et al., 2017; Murton et al., 2017) and this study. Photograph taken by Alexander Gabyshev in 2015.
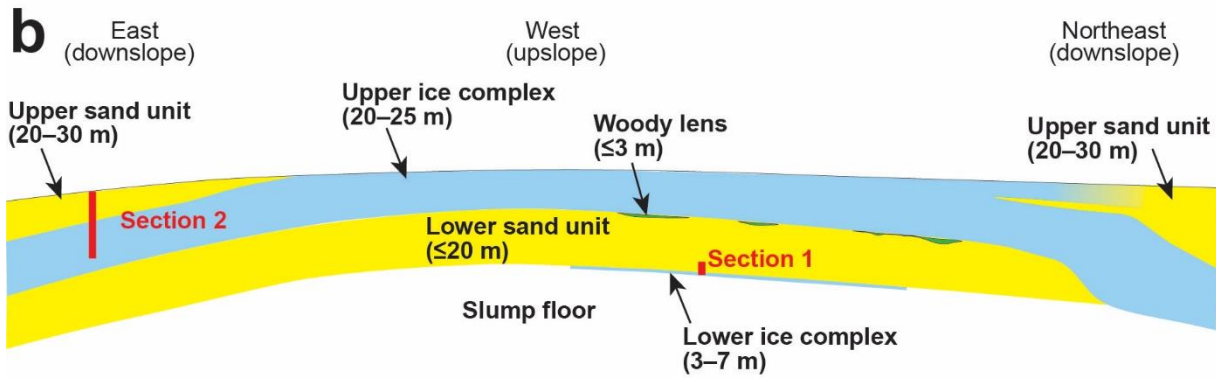
Figure 3. (a) Panoramic photograph of the Batagay megaslump with main stratigraphic units and approximate sampling locations of ice wedges (blue arrows). ~~Furthermore,~~R~~r~~ed circles and numbers indicate the approximate sampling locations of ice wedges used by (Vasil'chuk et al., 2017)~~.~~, (b) Schematic stratigraphic section of the exposed units along the headwall of the Batagay megaslump with approximate positions of the studied sections.
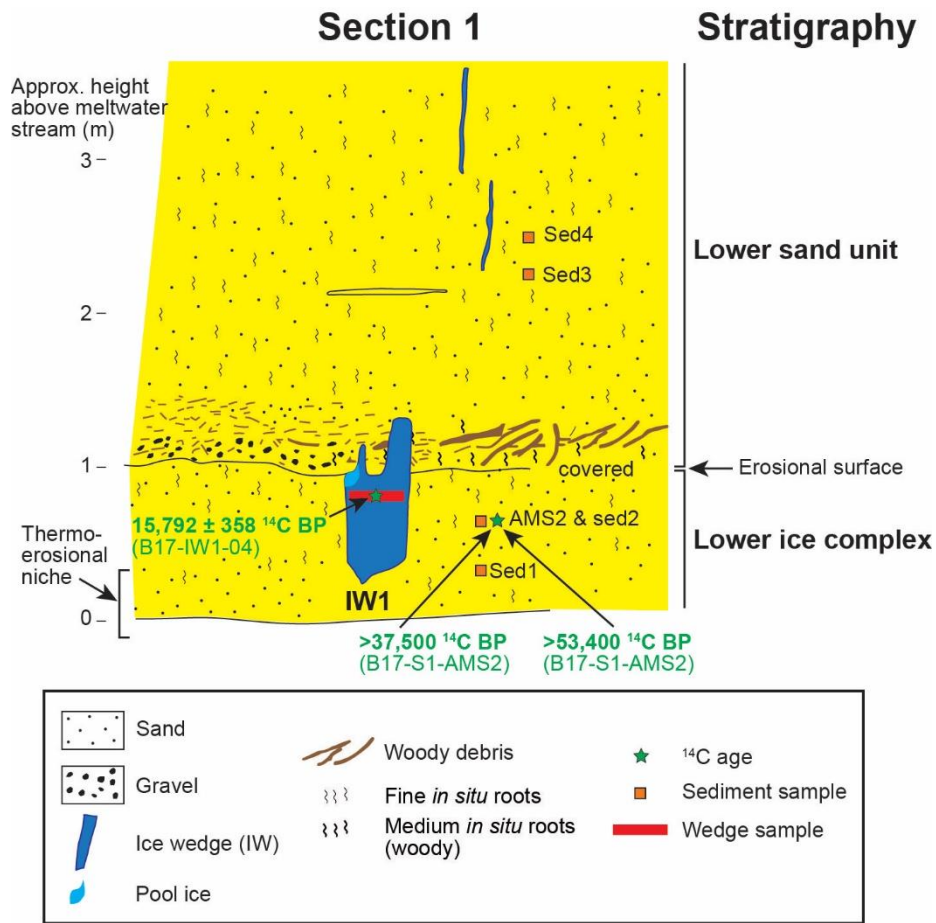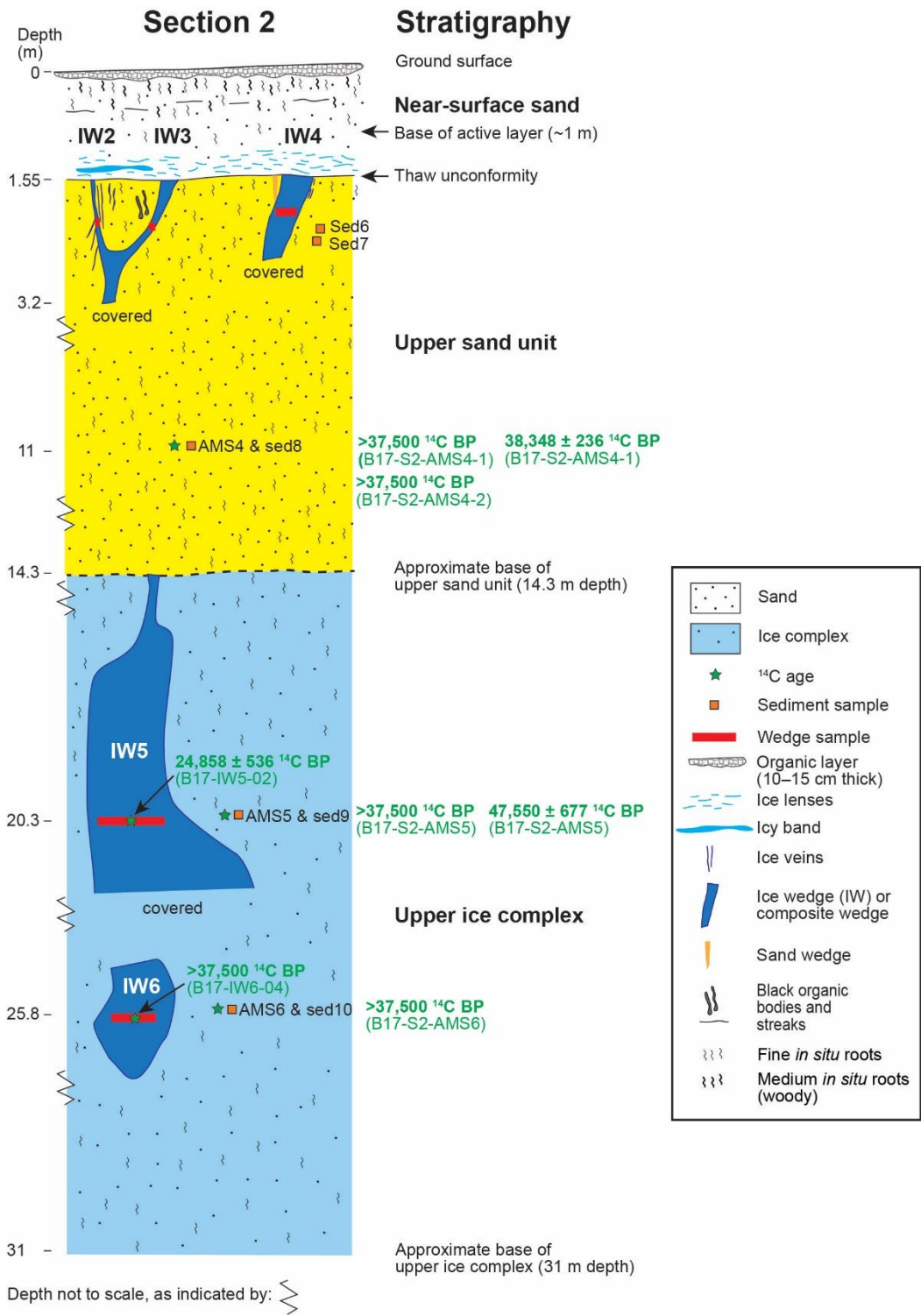
Figure 4. Schematic ~~cryostratigraphy~~ cryostratigraphic sketch of Section 1, Batagay megaslump.

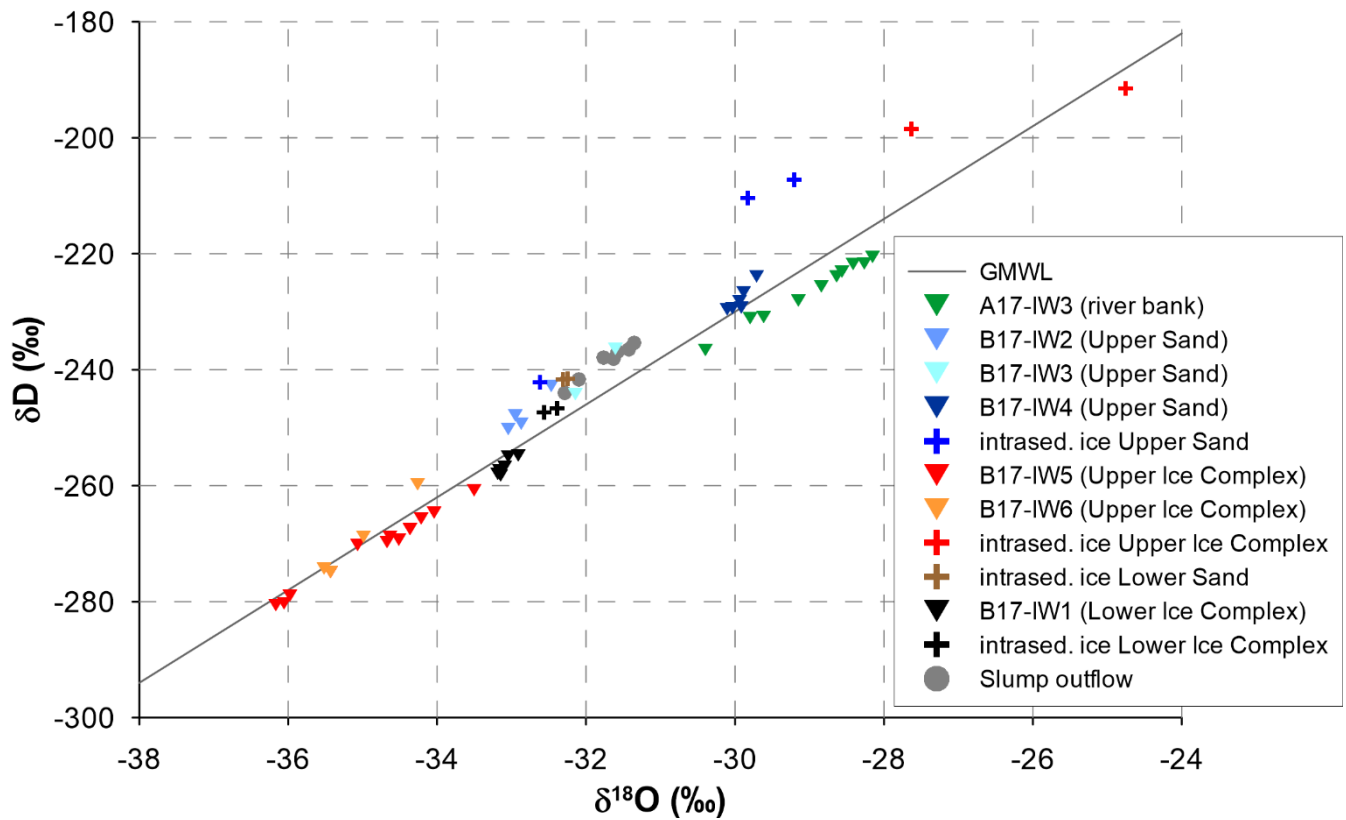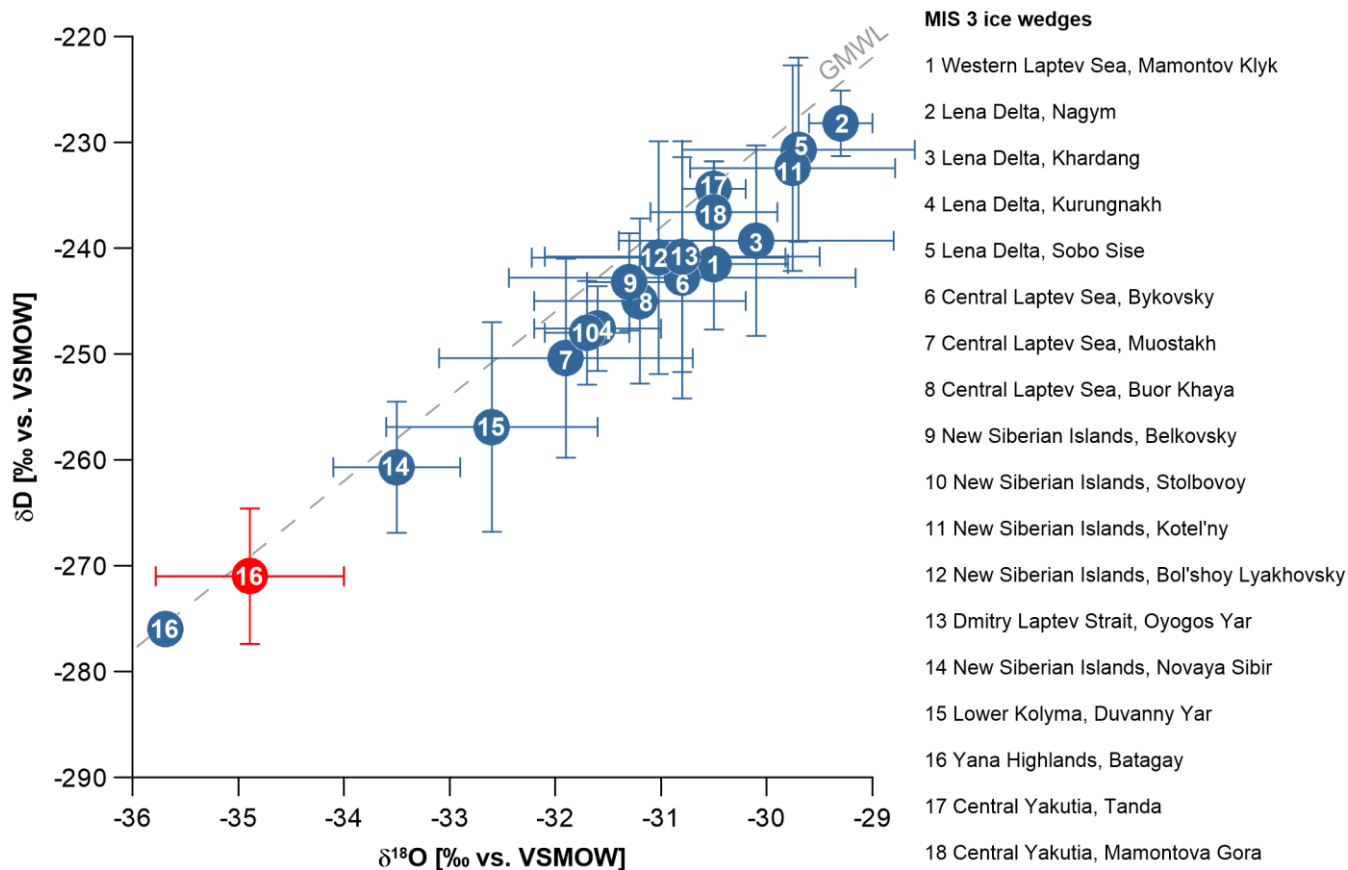**Figure 5.** Schematic ~~cryostratigraphy~~ cryostratigraphic sketch of Section 2, Batagay megaslump.

Figure 6. Co-isotopic $\delta^{18}O$—δD diagram of ice wedges and intrasedimental ice sampled at the Batagay megaslump and the Adycha River. ~~Furthermore, the~~ The data ~~of~~ from the Batagay megaslump outflow samples ~~are shown which display~~record an integrated signal of the entire Batagay permafrost sequence and modern precipitation.
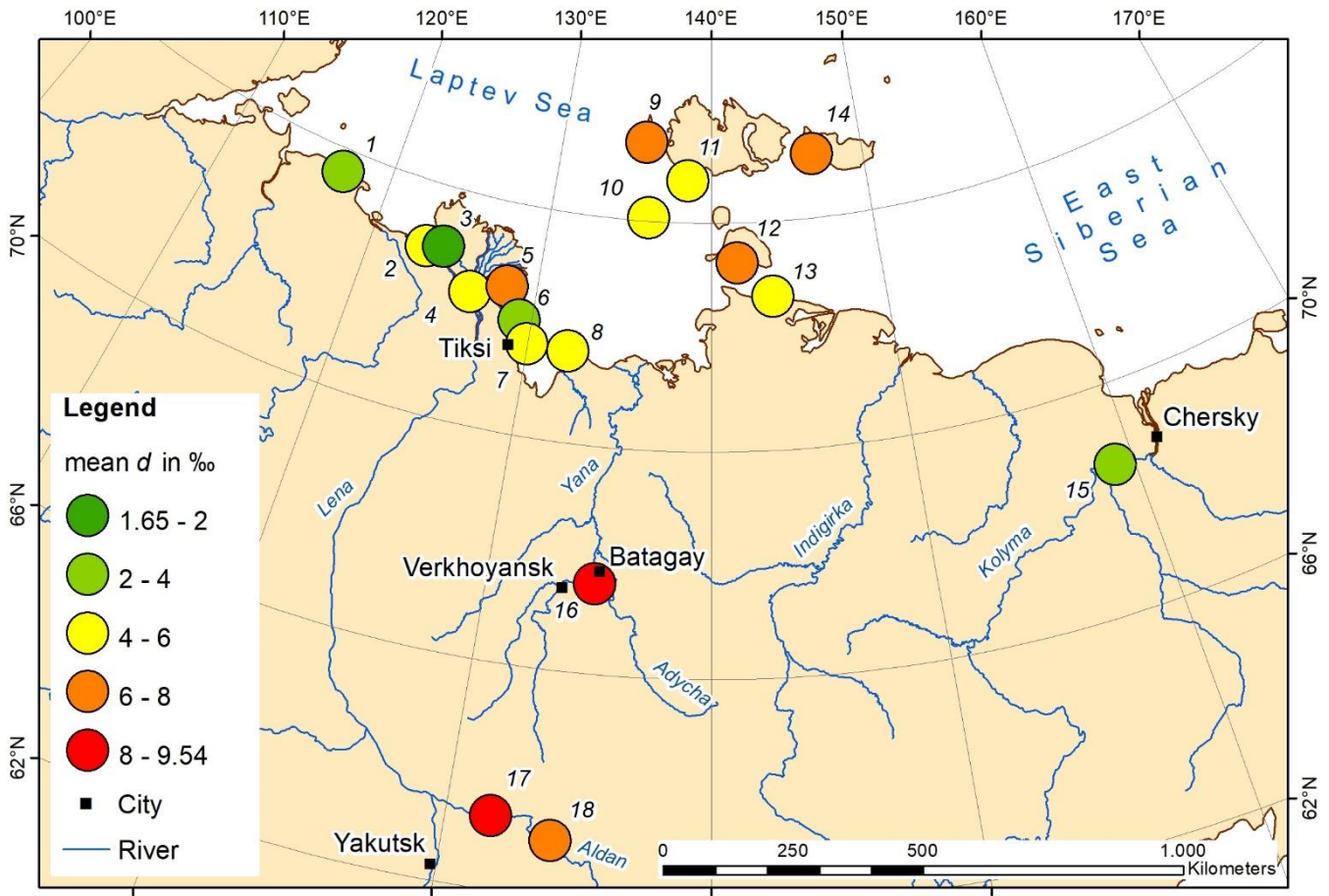
MIS 3 ice wedges

1 Western Laptev Sea, Mamontov Klyk
2 Lena Delta, Nagym
3 Lena Delta, Khardang
4 Lena Delta, Kurungnakh
5 Lena Delta, Sobo Sise
6 Central Laptev Sea, Bykovsky
7 Central Laptev Sea, Muostakh
8 Central Laptev Sea, Buor Khaya
9 New Siberian Islands, Belkovsky
10 New Siberian Islands, Stolbovoy
11 New Siberian Islands, Kotel'ny
12 New Siberian Islands, Bol'shoy Lyakhovsky
13 Dmitry Laptev Strait, Oyogos Yar
14 New Siberian Islands, Novaya Sibir
15 Lower Kolyma, Duvanny Yar
16 Yana Highlands, Batagay
17 Central Yakutia, Tanda
18 Central Yakutia, Mamontova Gora

Figure 7. Comparison of stable isotope data from Siberian ice wedges attributed to the ~~Kargin~~ MIS 3 interstadial (about 50 to 30 ~~ka~~kyr), comprising data from the ~~Western~~ western Laptev Sea (Magens, 2005), the Lena River Delta (Schirrmeister et al., 2003; Schirrmeister et al., 2011a; Wetterich et al., 2008; Opel, unpublished), the ~~Central~~ central Laptev Sea (Meyer et al., 2002a; Meyer/Opel, unpublished; Schirrmeister et al., 2017), the New Siberian Islands and the Dmitry Laptev Strait (Schirrmeister, unpublished; Wetterich et al., 2014; Opel et al., 2017b), the Kolyma Lowland (Strauss, 2010), the Yana Highlands (this study; Vasil'chuk et al., 2017), and ~~Central~~ central Yakutia (Schirrmeister, unpublished; Popp et al., 2006). Further information is given in Table ~~S2~~S3.
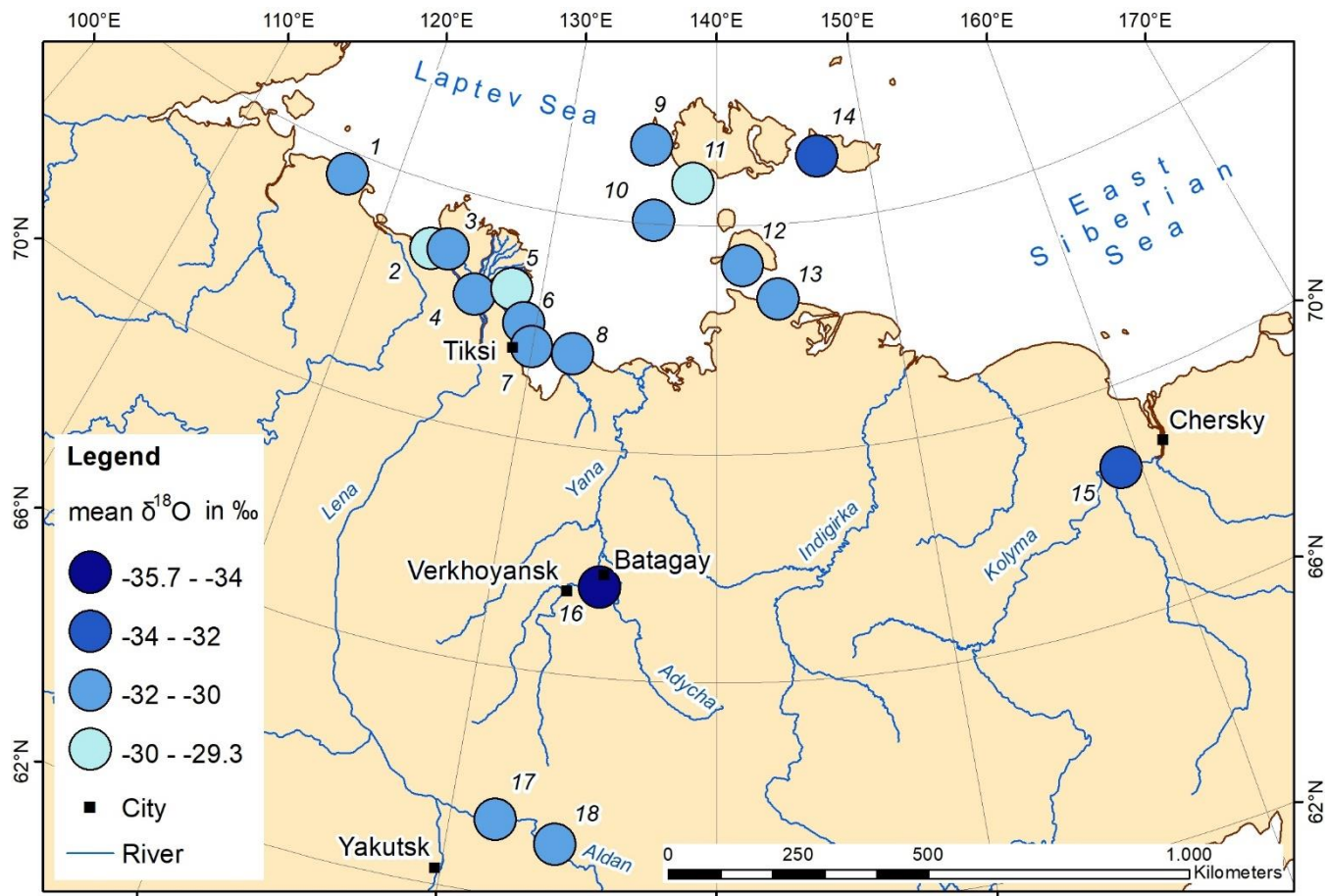
Figure 8. Map of mean δ¹⁸O data from Siberian ice wedges attributed to the ~~Kargin~~ MIS 3 interstadial (about 50 to 30 ~~ka~~kyr), Site IDs are given in **Figure 7** and further details in **Table** ~~S2~~S3.

5

Figure 9. Map of mean *d* data from Siberian ice wedges attributed to the ~~Kargin~~ MIS 3 interstadial (about 50 to 30 ~~ka~~kyr), Site IDs are given in **Figure 7** and further details in **Table** ~~S2~~S3.